Monthly Notices of the ROYAL ASTRONOMICAL SOCIETY
MNRAS **442,** 3044–3064 (2014) doi:10.1093/mnras/stu1099

The halo+cluster system of the Galactic globular cluster NGC 1851★

A. F. Marino,[1]† A. P. Milone,[1] D. Yong,[1] A. Dotter,[1] G. Da Costa,[1] M. Asplund,[1] H. Jerjen,[1] D. Mackey,[1] J. Norris,[1] S. Cassisi,[2] L. Sbordone,[3,4,5] P. B. Stetson,[6] A. Weiss,[7] A. Aparicio,[8,9] L. R. Bedin,[10] K. Lind,[11] M. Monelli,[8,9] G. Piotto,[10,12] R. Angeloni[13,14] and R. Buonanno[2]

[1]*Research School of Astronomy & Astrophysics, Australian National University, Mt Stromlo Observatory, via Cotter Rd, Weston, ACT 2611, Australia*
[2]*INAF–Osservatorio Astronomico di Teramo, via M. Maggini, I-64100 Teramo, Italy*
[3]*Zentrum für Astronomie der Universität Heidelberg, Landessternwarte, Königstuhl 12, D-69117 Heidelberg, Germany*
[4]*Millennium Institute of Astrophysics, Av. Vicuña Mackenna 4860, 782-0436 Macul, Santiago, Chile*
[5]*Pontificia Universidad Católica de Chile, Av. Vicuña Mackenna 4860, 782-0436 Macul, Santiago, Chile*
[6]*Herzberg Institute of Astrophysics, National Research Council Canada, 5071 West Saanich Road, Victoria, BC V9E 2E7, Canada*
[7]*Max-Planck-Institut für Astrophysik Karl-Schwarzschild-Str. 1, D-85741 Garching bei München, Germany*
[8]*Instituto de Astrofísica de Canarias, La Laguna, E-38200 Tenerife, Spain*
[9]*Departamento de Astrofísica, Universidad de La Laguna, E-38200 Tenerife, Spain*
[10]*INAF–Osservatorio Astronomico di Padova, Vicolo dell'Osservatorio 5, I-35122 Padova, Italy*
[11]*Institute of Astronomy, University of Cambridge, Madingley Road, Cambridge CB3 0HA, UK*
[12]*Dipartimento di Fisica e Astronomia 'Galileo Galilei', Università di Padova, Vicolo dell'Osservatorio 3, I-35122 Padova, Italy*
[13]*Department of Electrical Engineering, Center for Astro-Engineering, Pontificia Universidad Católica de Chile, Av. Vicuña Mackenna 4860, 782-0436 Macul, Santiago, Chile*
[14]*The Milky Way Millennium Nucleus, Av. Vicuña Mackenna 4860, 782-0436 Macul, Santiago, Chile*

Accepted 2014 June 1. Received 2014 May 30; in original form 2014 March 8

ABSTRACT

NGC 1851 is surrounded by a stellar component that extends more than 10 times beyond the tidal radius. Although the nature of this stellar structure is not known, it has been suggested to be a sparse halo of stars or associated with a stellar stream. We analyse the nature of this intriguing stellar component surrounding NGC 1851 by investigating its radial velocities and chemical composition, in particular in comparison with those of the central cluster analysed in a homogeneous manner. In total we observed 23 stars in the halo with radial velocities consistent with NGC 1851, and for 15 of them we infer [Fe/H] abundances. Our results show that (i) stars dynamically linked to NGC 1851 are present at least up to ∼2.5 tidal radii, supporting the presence of a halo of stars surrounding the cluster; (ii) apart from the NGC 1851 radial velocity-like stars, our observed velocity distribution agrees with that expected from Galactic models, suggesting that no other substructure (such as a stream) at different radial velocities is present in our field; (iii) the chemical abundances for the *s*-process elements Sr and Ba are consistent with the *s*-normal stars observed in NGC 1851; (iv) all halo stars have metallicities, and abundances for the other studied elements Ca, Mg and Cr, consistent with those exhibited by the cluster. The complexity of the whole NGC 1851 cluster+halo system may agree with the scenario of a tidally disrupted dwarf galaxy in which NGC 1851 was originally embedded.

Key words: techniques: imaging spectroscopy – globular clusters: general – globular clusters: individual: NGC 1851.

1 INTRODUCTION

Recent discoveries on multiple stellar populations in globular clusters (GCs) have revealed that some of these old stellar systems show chemical inhomogeneities, not just in the light elements involved in the hot H-burning, but also in heavier elements and in the overall metallicity. To explain the large metallicity dispersion in ω Centauri, it has been suggested that this GC is the remnant of a dwarf galaxy

★Based on data collected at the European Southern Observatory with the FLAMES/GIRAFFE spectrograph, under the programmes 088.A-9012 and 084.D-0470. Based also on observations made with MPG 2.2 m telescope at the La Silla Paranal Observatory under the programmes 085.A9028(A) and 088.A9012(A).

† E-mail: amarino@mso.anu.edu.au

disrupted through tidal interactions with the Milky Way, rather than a true GC (e.g. Norris, Freeman & Mighell 1996; Bekki & Freeman 2003; Bekki & Norris 2006). In this scenario, ω Centauri would be the dense nucleus of a dwarf galaxy, which was cannibalized by the Milky Way. The recent discoveries of more ω Centauri-like GCs, with internal metallicity variations (e.g. Da Costa et al. 2009, 2014; Marino et al. 2009; Yong et al. 2014), support the hypothesis that at least these 'anomalous' GCs were as massive as small galaxies capable of retaining fast supernova ejecta. The relatively high fraction of metal richer stars in these GCs also supports the idea that they were more massive. The possible GC–dwarf galaxy connection may have consequences for near-field cosmology and the hierarchical assembly of our Galaxy. At least the GCs with internal variations in metallicity may contribute to the inventory of original satellites, along with existing dwarf spheroidals and ultra-faints, to alleviate the 'missing satellites' problem of the Λ cold dark matter scenario (e.g. Kauffmann, White & Guiderdoni 1993; Klypin et al. 1999; Moore et al. 1999).

The hypothesis that at least some GCs may constitute the surviving nuclei of tidally disrupted dwarf galaxies implies that the Milky Way has stripped the less bound external stars from these systems during successive passages through the Galactic potential, leaving only their compact nuclei. A snapshot of this phenomenon may be M54, as it shows an intrinsic Fe dispersion (Bellazzini et al. 2008; Carretta et al. 2010) and lies at the centre of the Sagittarius dwarf galaxy that is being tidally disrupted by the Milky Way (Ibata, Gilmore & Irwin 1994).

While nearly all the Galactic GCs have chemical variations in the light elements involved in the hot H-burning (such as C, N, O, Na; see e.g. Kraft 1994; Gratton, Sneden & Carretta 2004), only a few of them are known to possess spreads in Fe and *s*-element abundances (ω Cen, M22, NGC 1851, M2, NGC 5824, NGC 3201; e.g. Smith et al. 2000; Yong & Grundahl 2008; Da Costa et al. 2009; Marino et al. 2009, 2011a,b; Yong et al., 2014; Da Costa, Held & Saviane 2014; Lardo et al. 2013; Simmerer et al. 2013). It is intriguing that the GCs with metallicity and *s*-element variations are generally the more massive ones. The complexity of the multiple stellar populations in these objects is puzzling and we do not have yet a coherent picture to explain the formation of their different generations of stars.

In this context, NGC 1851 is one of the most intriguing targets. Much effort has been dedicated to this GC after the discovery of a prominent bimodal subgiant branch (SGB; Milone et al. 2008). The formation scenario for these two SGB components is still under debate. Observational constraints for the sequence of events that led to the formation of these stellar groups can be inferred from their chemical compositions and their radial distributions in the cluster. The radial profile of the two SGB components has been found to not change significantly within 8 arcmin from the cluster centre (Milone et al. 2009). In contrast, Zoccali et al. (2009) did not observe the faint SGB (fSGB) out to ∼2.4 arcmin in the south-west quadrant.

By analysing high-resolution Ultraviolet and Visual Echelle Spectrograph (UVES) spectra for NGC 1851 red giants (RGB), Yong & Grundahl (2008) discovered that this cluster hosts two groups of stars with different content of *s*-process elements (see also Carretta et al. 2010; Villanova, Geisler & Piotto 2010). These two stellar groups have been found to define two RGB sequences following on from the two different SGBs (Han et al. 2009; Lee et al. 2009; Lardo et al. 2012). The photometric split on the SGB observed by Milone et al. (2008) has been theoretically interpreted as due to either a difference in age of ∼1 Gyr or to a possible dichotomy in the C+N+O (Cassisi et al. 2008; Ventura et al. 2009; Sbordone et al. 2011). The latter scenario has been supported by spectroscopic studies showing that *s*-enriched stars are also enhanced in their overall C+N+O content (Yong et al. 2009; Yong et al., 2014). We note, however, that Villanova et al. (2010) did not find an abundance spread for C+N+O. To date, variations in the overall C+N+O have also been found in other two 'anomalous' GCs, M22 (Marino et al. 2011a, 2012a; Alves-Brito et al. 2012) and ω Centauri (Marino et al. 2012b).

Interestingly, NGC 1851 is surrounded by a diffuse stellar halo with a radius of more than 250 pc (67 arcmin from the cluster centre) and a mass of about 0.1 per cent of the dynamical mass of NGC 1851 (Olszewski et al. 2009). The extension of this stellar structure is far beyond the tidal radius predicted by the King model (King 1962), that is the distance from the cluster centre where cluster stars are expected to drastically disappear due to tidal interactions.

The origin of this halo remains unknown, although various hypotheses exist. It could be the consequence of isolated cluster evaporation through tidal or disc shocking that may have originated a stellar tail. Such processes are believed responsible for the streams observed in several GCs, such as Pal 5 (Odenkirchen et al. 2001; Koch et al. 2004). Observations of NGC 1851 are contradictory: while photometrically there is no evidence for tidal streams (Olszewski et al. 2009), the presence of a possible tail of stars with radial velocity (RV) around ∼150 km s^{-1} has been reported by Sollima et al. (2012).

Alternatively, the huge halo of NGC 1851 could have formed from the destruction of a dwarf galaxy in which the cluster may have once been embedded. Bekki & Yong (2012) outlined a possible self-consistent and dynamically plausible scenario for the formation of NGC 1851's multiple populations and its stellar halo. In their scenario, two GCs in a dwarf galaxy merge (owing to the low velocity dispersion of the host dwarf) and form a new nuclear star cluster surrounded by field stars of the host dwarf. The host dwarf galaxy is stripped through tidal interaction with the Milky Way leaving the stellar nucleus which is observed as NGC 1851. Thus, the two stellar populations in NGC 1851 originate in the two GCs that merged to form the nucleus. Bekki & Yong (2012) predict that NGC 1851's stellar halo contains three stellar populations: two from the original GCs that merged to form the nucleus and the remaining population is from field stars surrounding stellar nuclei.

In the present study, we investigate the nature of this intriguing stellar system, the GC NGC 1851 plus its halo, by deriving RVs and, for the first time, chemical abundances for the halo stars. The chemical and dynamical properties of the halo stars will be compared with the ones observed within the tidal radius of the cluster.

2 DATA

Basic information for NGC 1851 can be found in Harris (1996, 2010 edition, and references therein). Its distance from the Sun is ∼12.1 kpc. The King tidal radius of NGC 1851 was estimated to be 6.7 arcmin by McLaughlin & van der Marel (2005), which is lower than the value of 11.7 arcmin in the previous Harris compilation derived by Trager, Djorgovski & King (1993). Given the large uncertainties related to the determination of the tidal radius, we assume in this work the conservative value of 11.7 arcmin. Assuming the M_V from Harris (2010 edition) and a typical $M/L_V = 1.6$, we get a mass of $M \approx 10^{5.45}$ M$_\odot$, which places NGC 1851 among the most massive GCs. We assumed for the centre of the cluster the coordinates (RA; Dec.)$_{J2000}$ = (05:14:06.76; −40:02:47.6) from Goldsbury et al. (2011).

Table 1. Description of the photometric images used for the first time in this work.

Telescope	Camera	Filter	Exposure time	Field	Date	Programme	PI
Max Planck 2.2 m, La Silla	WFI	*U*	8× ∼800 s	Inner	2012 February 22–26	088.A9012(A) (SUMO)	A. F. Marino
Max Planck 2.2 m, La Silla	WFI	*B*	2× ∼300 s+6× ∼150 s	Outer	2012 February 26–28	088.A9012(A) (SUMO)	A. F. Marino
Max Planck 2.2 m, La Silla	WFI	*V*	8× ∼300 s	Outer	2013 November 13	085.A9028(A)	R. Gredel
Max Planck 2.2 m, La Silla	WFI	*I*	3× ∼120 s+4× ∼250 s	Outer	2012 February 26–28	088.A9012(A) (SUMO)	A. F. Marino

2.1 The photometric data set

In this paper, we used four distinct photometric data sets. First, we used Stetson (2000) ground-based *B*, *V*, *R* and *I* photometry. This photometric catalogue has been established from about 550 images taken at different telescopes, i.e. the Max Planck 2.2 m, the Cerro Tololo Inter-American Observatory (CTIO) 4, 1.5 and 0.9 m telescopes, and the Dutch 0.9 m telescope in La Silla. These data have been reduced by using procedures for the photometric and astrometric data reduction described by Stetson (2005), and have already been used in Milone et al. (2009). We refer the reader to section 2.3 of Milone et al. (2009) for further information on this data set. In the present work, we have complemented the Stetson catalogue with images collected with the Wide Field Imager (WFI) of the Max Planck 2.2 m telescope at La Silla (WFI@2.2m) through the *U* filter under the SUrvey of Multiple pOpulations (SUMO) campaign. Details on the WFI data in the *U* band, analysed here for the first time, are provided in Table 1. In summary, *UBVRI* photometry has been used for stars in a region between ∼10 arcmin to the south and 13 arcmin to the north, and between ∼15 arcmin to the west and 15 arcmin to the east, relatively to the centre of NGC 1851.

Secondly, to study stars in the halo of NGC 1851, we collected *BVI* images with WFI@2.2m of a field between ∼10 and 35 arcmin to the south of the cluster centre. Photometry and astrometry for this data set have been obtained by using the program img2xym_WFI and the procedure described by Anderson et al. (2006). Details of the WFI@2.2m data set, which has been analysed for the first time in this paper, are listed in Table 1.

Third and finally, to investigate the most crowded central regions, we use *Hubble Space Telescope* (*HST*) *F*606*W* and *F*814*W* photometry obtained with the Wide Field Channel of the Advanced Camera for Survey (WFC/ACS) and *F*275*W* photometry collected with the Ultraviolet and Visual Channel of the Wide Field Camera 3 (UVIS/WFC3). The WFC/ACS photometry comes from GO-10775 (PI: A. Sarajedini; see Sarajedini et al. 2007 and Anderson et al. 2008) and is presented in Milone et al. (2008). The UVIS/WFC3 photometry comes from GO-12311 (PI: G. Piotto) and is presented in Piotto et al. (2012, see also Bellini et al. 2010 for details on the data reduction).

We adopt the following terminology for the various fields for which different photometries are available: (1) 'central field' for the field of 3 arcmin × 3 arcmin covered by the *HST* photometry; (2) 'inner field' is all the field inside the tidal radius, e.g. *HST* photometry where available, Stetson+SUMO photometry otherwise; (3) 'outer field' is the field outside the tidal radius.

The left- and right-hand panels of Fig. 1 show the inner and outer field *V* versus $(B - I)$ colour–magnitude diagrams (CMDs). On each CMD, we superimpose the fiducial line of the cluster. The inner and outer field CMDs have not been de-reddened. However, the reddening across the NGC 1851 field of view is very low, $E(B - V) = 0.02$, and the differential reddening should not be significant as it is much lower than internal uncertainties in the ground-based photometry. The reddening variation across a field of $2^\circ \times 2^\circ$ around the cluster centre predicted from the Schlegel, Finkbeiner & Davis (1998) maps is also low with minimum and maximum values for $E(B - V)$ of 0.0287 and 0.0351, respectively. A maximum reddening variation of 0.0064 mag does not produce significant colour changes to the inner and outer field CMDs. The location on the sky of the ground-based photometry fields, as well as the central *HST* field, relative to the cluster centre, is represented in the middle panel: the central *HST* field is delimited in red; the region that we define 'inner field' is located within the tidal radius, represented as a green circle; while the region defined as 'outer field' is comprised within the cyan square.

Ground-based photometric data have been used to estimate atmospheric parameters, as described in Section 4.1. Hence, it is important to have an estimate of the internal photometric uncertainties. According to the photometric catalogues from Stetson (2000), the average σ(mag) for a star with $V \sim 19.5$ in the *B*, *V*, *R*, *I* bands is ∼0.003, ∼0.002, ∼0.012, ∼0.003 mag, respectively. Since each star has been typically observed in tens of images, the formal error should be significantly smaller. In the external field, we obtained *B*, *V*, *I* formal errors of ∼0.005, ∼0.004, ∼0.006 mag, respectively. Such small values are lower limits of the true photometric errors as demonstrated by the fact that the colour spread of all the sequences of the CMDs is significantly larger than few millimagnitudes. Photometry is indeed affected by a number of additional uncertainties. Spatial variations of the photometric zero-point along the field of view, introduced by small inaccuracy in the point spread function model, by the sky or bias determination, or by small reddening variations, are a very common property of any photometric catalogue (see Anderson et al. 2008 for a discussion on this issue). To estimate the error of target stars, we started by measuring the colour spread of main sequence (MS) stars as described in Milone et al. (2009, see their section 6). Briefly, we have verticalized the MS of NGC 1851 by subtracting to the colour of each star the colour of the MS at the same *V* magnitude, and then we have determined the histogram distribution of the colour difference (Δcolour), and, finally, we have fitted the histogram with a Gaussian. We have repeated this procedure for $(B - I)$, $(V - I)$, $(R - I)$ and $(V - I)$ colours. We assumed the σ of the least-squares best-fitting Gaussian as our estimate of the colour error. Specifically, to estimate the errors associated with SGB stars in the central field, we used the colour spread of MS stars with $19.2 < V < 19.4$. We obtained $\sigma_{B-I} = 0.030$, $\sigma_{B-R} = 0.031$, $\sigma_{B-V} = 0.024$, $\sigma_{V-I} = 0.024$. We thus assumed 0.02 as typical magnitude uncertainty for stars in the internal field. In the case of stars in the external field, due to the small number of MS stars, we used a larger magnitude interval ($19.4 < V < 20.4$) and accounted for field-star contamination by subtracting from the observed histograms of Δcolour distribution the corresponding histogram distributions for field stars. The latter has been determined by using the Besançon Galactic model (Robin et al. 2003) for stars within the same area as the external field. We found $\sigma_{B-I} = 0.035$, $\sigma_{B-V} = 0.031$, $\sigma_{V-I} = 0.032$, and thus assumed

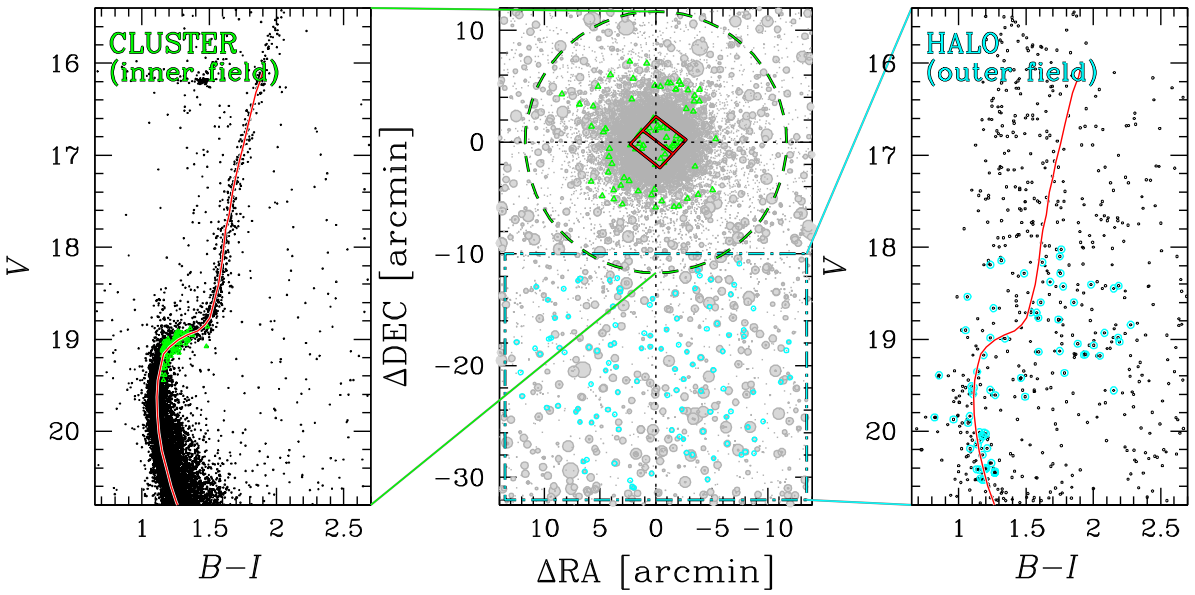

Figure 1. Location of the spectroscopic targets in RA and Dec. (central panel). The NGC 1851 stars in the cluster (inner field) have been plotted in green and are within the tidal radius (green dashed circle). Stars in the halo have been plotted in cyan and are contained in the outer WFI field delimited by the cyan dashed line. The footprint of the ACS/WFC field has been delimited in red. In the two sided panels, we represent the V versus $(B - I)$ CMDs for stars in the inner and outer fields, with the corresponding position of our spectroscopic targets. Red lines are the fiducials of the cluster CMD.

a typical magnitude uncertainty of 0.02 mag in each filter. These uncertainties will be considered when discussing the impact of photometric errors on the atmospheric parameters (see Section 4.1).

2.2 The spectroscopic data set

Our spectroscopic data consist of FLAMES/GIRAFFE spectra (Pasquini et al. 2002) observed under the programme 090.D-0687A (PI: A. P. Milone) taken with no simultaneous calibration lamp. The low-resolution LR02 GIRAFFE setup was employed, which covers a spectral range of ∼600 Å from 3964 to 4567 Å, and provides a resolving power $R \equiv \lambda/\Delta\lambda$ ∼6400. All our target halo stars, for which we aim to obtain kinematical and chemical information, were observed in the same FLAMES plate in 25 different exposures of 46 min, for a total integration time of ∼19 h.

The large amount of observing time, the multi-object capability of FLAMES and the low resolution were crucial to observe mostly very faint stars. In fact, we wanted to find the largest possible number of stars associated with NGC 1851 in a field of 30 arcmin × 30 arcmin outside the tidal radius of the cluster, mostly populated by field stars. Hence, our observations concentrated on the fainter but more densely populated regions of the CMD where the resolution of the low-resolution GIRAFFE settings (∼6000) is the limit to get decent signal in a reasonable amount of observing time.

The signal-to-noise ratio (S/N) of the fully reduced combined spectra varies from star to star. It not only depends on the luminosity of the targets but also on the efficiency of the fibres. Among the stars for which we inferred chemical abundances, the maximum S/N is ∼50 per pixel for the more luminous stars that are starting to ascend the RGB; the S/N decreases for MS stars. We impose a limit of S/N ∼15 on the spectra of the outer field from which we infer chemical abundances. Of course, the number of analysed spectral lines, and hence elements, increases with the S/N.

To supplement our halo star sample, we analysed data from the archive for the internal field of NGC 1851. This sample for the internal field has already been analysed by Gratton et al. (2012, hereafter G12). We decided to re-analyse these data to ensure an optimal comparison sample as it consists of SGB stars for NGC 1851 observed with the same FLAMES/GIRAFFE setup (LR02) as our NGC 1851 halo stars. A homogeneous comparison of the chemical contents of the halo stars with those obtained for the internal field of NGC 1851 (within the tidal radius) is crucial to understand if the halo of NGC 1851 shares similar abundances with the cluster. The fully reduced spectra for the stars in the internal field have S/N of around 50.

The position on the sky and on the $V - (B - I)$ CMD of our spectroscopic targets is shown in Fig. 1. In the following, we will refer to the stars outside the tidal radius of NGC 1851 as NGC 1851 halo or external field stars; the internal field stars (within the tidal radius) will be called NGC 1851 cluster stars; while all the other stars in the external field that do not share the RV of NGC 1851 will be simply considered field stars (see Section 3). A list of all the analysed stars (cluster+halo) and their basic photometric data is provided in Table 2.

All the data were reduced in the same manner. The reduction, involving bias subtraction, flat-field correction, wavelength calibration and sky subtraction, was done with the dedicated pipeline BLDRS v0.5.3.[1] RVs for both external and internal field stars were derived using the IRAF@FXCOR task, which cross-correlates the object spectrum with a template. For the template, we used a synthetic spectrum obtained through the spectral synthesis code SPECTRUM (Gray & Corbally 1994).[2] This spectrum was computed with a model stellar atmosphere interpolated from the Castelli & Kurucz (2004) grid, adopting parameters (effective temperature, surface gravity, microturbulence, [Fe/H]) = (6000 K, 3.5, 1.0 km s^{-1}, −1.20). The cross-correlation function was fitted with a Gaussian profile. We used the entire observed wavelength range to

[1] See http://girbld-rs.sourceforge.net

[2] See http://www.phys.appstate.edu/spectrum/spectrum.html for more details.

Table 2. Coordinates, basic photometric data and RVs for the NGC 1851 halo and cluster (inner field) stars. The full versions will be available online as supplementary material.

ID	RA	Dec.	*B*	*V*	*R*	*I*	*F*606*W*	*F*814*W*	RV (km s^{-1})	SGB
					Halo					
T119	05:14:08.280	−40:16:48.000	19.909	18.843	–	17.631	–	–	98.924	Field
T198	05:13:47.160	−40:14:14.200	19.399	18.711	–	17.820	–	–	319.500	Uncertain
T105	05:13:56.870	−40:18:34.600	18.935	17.872	–	16.855	–	–	50.489	Field
					Cluster					
SGB-a.10	05:14:14.390	−40:02:56.101	19.543	19.032	18.648	18.322	18.805	18.273	319.579	bSGB
SGB-a.12	05:14:13.250	−40:03:22.201	19.496	18.957	18.604	18.234	18.803	18.283	325.908	bSGB
SGB-a.13	05:14:12.630	−40:03:05.501	19.483	18.946	18.334	18.220	18.798	18.271	326.645	bSGB

cross-correlate the spectra with the template, which includes hydrogen lines. The choice of including hydrogen lines, which can increase internal uncertainties, was due to the low S/N of some single-exposure spectra for the halo stars. For the stars with higher S/N, we have weaker lines available for the cross-correlation, but to ensure homogeneity in the RV determination, we analyse all the spectra at the same manner and use the entire available spectral range. In any case, the dispersion of the RV measurements from different exposures for each star is indicative of our internal error (see Section 3).

Observed RVs were finally corrected to the heliocentric system.

In total we gathered spectra for 110 candidate NGC 1851 halo stars, spanning a wide range in both magnitude and colour. In the selection of the targets, we maximize the number of stars close to the NGC 1851 photometric sequences in order to increase the chance to observe NGC 1851 halo stars. We have also observed stars at larger distances from the NGC 1851 sequence to explore the possibility of having stars dynamically linked to the cluster, but with possible different chemistry.

3 RADIAL VELOCITIES

RVs have been obtained as explained in Section 2.2 from the individual exposures, and then simply averaged to get the final values for each star listed in Table 2. The internal errors associated with our mean RV values depend on the luminosity of the stars. They are higher for dwarfs with lower S/N.

In the inner field, the average error[3] from the distribution of the RV values obtained from different exposures is 0.49 ± 0.02 km s^{-1} (rms = 0.20 km s^{-1}). Only two stars (SGB-b-St.24 and SGB-b-St.4), both in the fSGB, have errors that are more than a 3σ level larger than the mean value. However, as these two stars are among the fainter stars in our inner field sample, their larger errors are likely due to the lower S/N of their spectra, rather than to binarity. The lack of outliers with large RV rms values for the stars analysed in the inner field suggests that there is no evidence for binaries in this sample. We note that we do not expect a large fraction of binaries in our inner field sample. Indeed, we note that the fraction of MS–MS binaries measured in the ACS field outside the half-mass radius is 1.6 ± 0.6 per cent (Milone et al. 2012).

In the outer field (total sample of 110 stars), the rms values in the RV distributions span a wide range. In some cases, the larger values are due to the low S/N of the low-luminosity star spectra; for some cases with good quality spectra, the large rms may reflect binarity. However, we prefer to not enter into much detail regarding this issue because we are interested exclusively in the subsample of outer field stars with RV compatible with NGC 1851. For this particular subsample of stars, the errors in RVs range from 0.47 to 7.8 km s^{-1}, decreasing with the S/N. In most cases, the error is as large as $\gtrsim$2 km s^{-1} so we cannot draw conclusions on the possible presence of binaries in our halo sample, especially for the fainter stars. Concluding, the internal error in RV for the outer field stars is typically high, preventing a secure assessing of the presence of binaries in this sample. We only can note that, if these halo stars belong to NGC 1851, due to the equipartition of energy, the binary fraction should be lower than that in the central field.

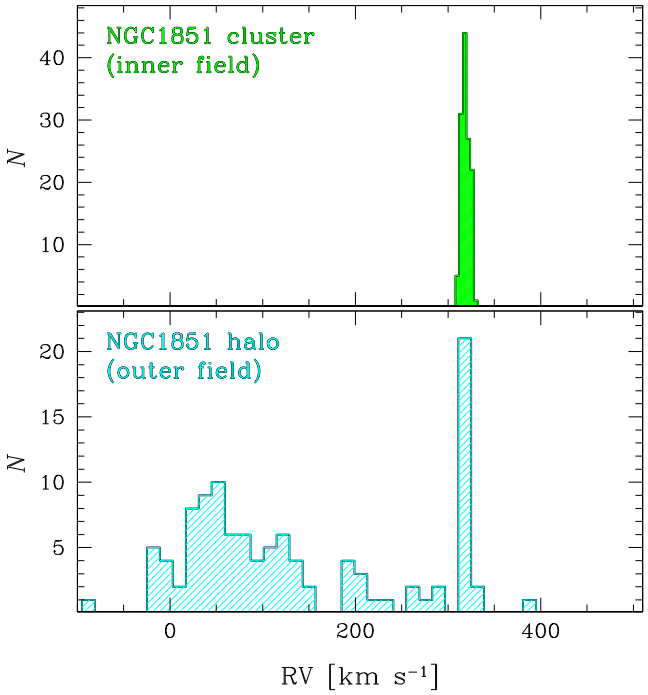

Figure 2. Lower panel: histogram distribution of RVs for the 110 stars in the outer field. Upper panel: histogram distribution of RVs for inner field stars.

In Fig. 2, we summarize our results for RVs obtained for stars in the inner (upper panel) and the outer field (lower panel). Inner field stars are clustered around an average RV value of $+319.5 \pm 0.5$ km s^{-1} (rms = 4.4 km s^{-1}), which is similar to previous estimate for NGC 1851 SGB stars of 318.2 ± 0.5 km s^{-1} (rms = 4.3 km s^{-1}) and 320.0 ± 0.4 km s^{-1} (rms = 4.9 km s^{-1}), from G12 and

[3] The error is assumed to be equal to the rms of the RVs obtained from each exposure divided by the square root of the number of exposures minus one.

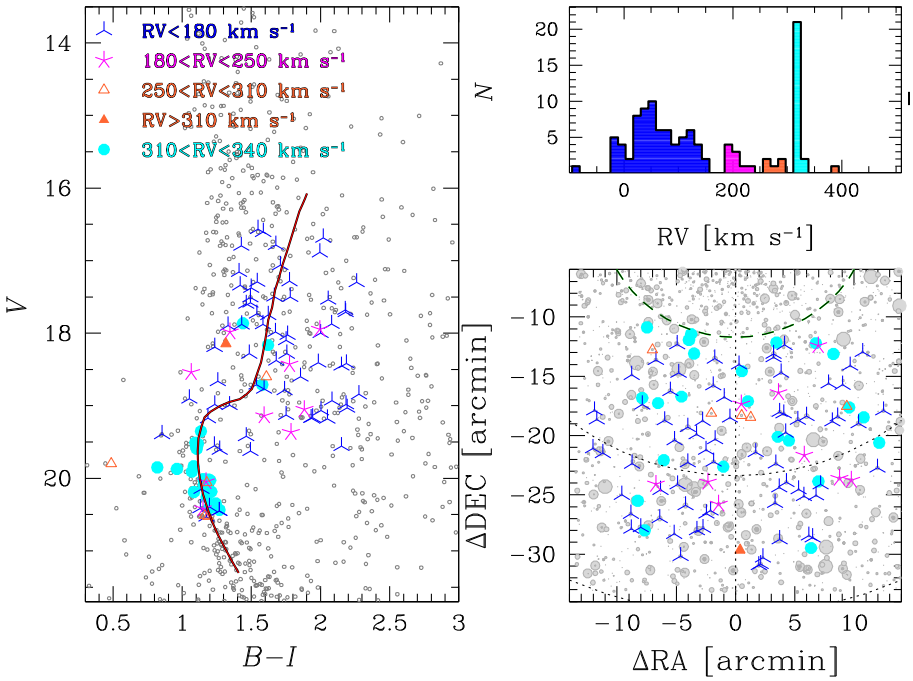

Figure 3. Left-hand panel: V versus $(B - I)$ CMD of stars in the outer field. Spectroscopic targets are represented with coloured symbols, according to their RV as indicated in the upper left and in the RV histogram distribution in the upper-right panel. Right-hand lower panel: spatial distribution of target stars in the halo. We mark with dashed green circle the tidal radius of NGC 1851. The dotted circles correspond to two and three times the tidal radius.

Scarpa et al. (2011), respectively. The RVs of the internal field stars suggest that all the analysed targets are likely cluster members as also supported by their position on the CMD (Fig. 1).

Due to the high contamination from the field, in contrast with what is observed in the inner region, the RV histogram of stars in the external field is complex. Most of the stars have RV $\lesssim 200$ km s^{-1} and define a broad distribution peaked at RV ≈ 50 km s^{-1}; then we observe a narrow peak around the same RV of NGC 1851, 14 stars at intermediate values, and one star with a very high radial velocity of RV $= 381.3$ km s^{-1}. The peak around the mean RV of NGC 1851 comprises 23 stars, and their average RV is $+318.4 \pm 1.0$ km s^{-1} (rms $= 4.9$ km s^{-1}).

Since NGC 1851 has a distinct RV in this Galactic sightline, members of its stellar halo should share its unambiguous kinematic signature. Hence, the presence of stars with RVs compatible with the cluster strongly supports the presence of a halo extending beyond the tidal radius of NGC 1851. To further support the existence of this halo, in Fig. 3 we analyse the spatial distribution and the position in the CMD of stars with different RVs. We have defined four groups of stars corresponding to different RV intervals. The RV histograms for the four groups of stars are plotted in the upper-right panel of Fig. 3. The location of these stars in our analysed field is represented in the lower-right panel of Fig. 3.

We note that the majority of stars with cluster-like RVs are distributed along the fiducial line of NGC 1851 (red line in the left-hand panel), in contrast with most of the stars with RV < 250 km s^{-1}, which span a broad interval of colour. This finding further supports the possibility that the group of cyan stars belongs to a halo surrounding NGC 1851. The colour and magnitude of four out of five stars with $250 <$ RV < 310 km s^{-1} are consistent with those of NGC 1851. However, we anticipate that a similar number of stars with these RVs and in this region of the CMD is expected from Galactic models (see the following section for details).

3.1 Comparison with a Galactic model

To investigate whether the peak at RV $\approx$320 km s^{-1} observed in Fig. 2 is associated with the halo of NGC 1851 or not, we compare our observations with the Galactic model by Robin et al. (2003).

The upper-left panel of Fig. 4 shows the synthetic V versus $(B - I)$ CMD for the ∼6100 stars that, according to the Besançon model (Robin et al. 2003), are located in a 60 arcmin × 60 arcmin region with the same coordinates as the field analysed here. The histogram and the kernel-density distributions of RVs for the stars are shown in the lower-left panel. The model generates population realizations based on probability as a function of the specific position in the parameter space.

A visual inspection of the CMD in the upper-left panel reveals that, as expected, stars with different velocities populate different regions of the CMD. Low-velocity stars (RV < 180 km s^{-1}), mainly dwarfs, define a broad sequence, mainly populated by disc stars, which is characterized by a large colour spread ($1 \lesssim (B - I) \lesssim 4$) and extends up to bright luminosities ($V < 14$). Most of the stars with high velocities (RV >180 km s^{-1}) populate a narrower sequence ($1 \lesssim (B - I) \lesssim 2$) and have, on average, lower luminosities.

However, we note that the sample of stars analysed here is located in a limited region of the CMD. In fact, to properly compare RVs of the observed stars and those from the Galactic model, we need to select a sample of stars in the synthetic CMD with almost the same colour and magnitude as the observed stars.

To this aim, we associated with each observed star the star in the Galactic-model CMD at the smallest 'distance' as suggested by Gallart et al. (2003, see their section 4) and Moni Bidin et al. (2011).

This distance is assumed as $d = \sqrt{(k \times (B - I))^2 + V^2}$, where k is a factor enhancing the difference in colour with respect to the magnitude difference. Our procedure to estimate the factor k appropriate for our data set comprises different steps.

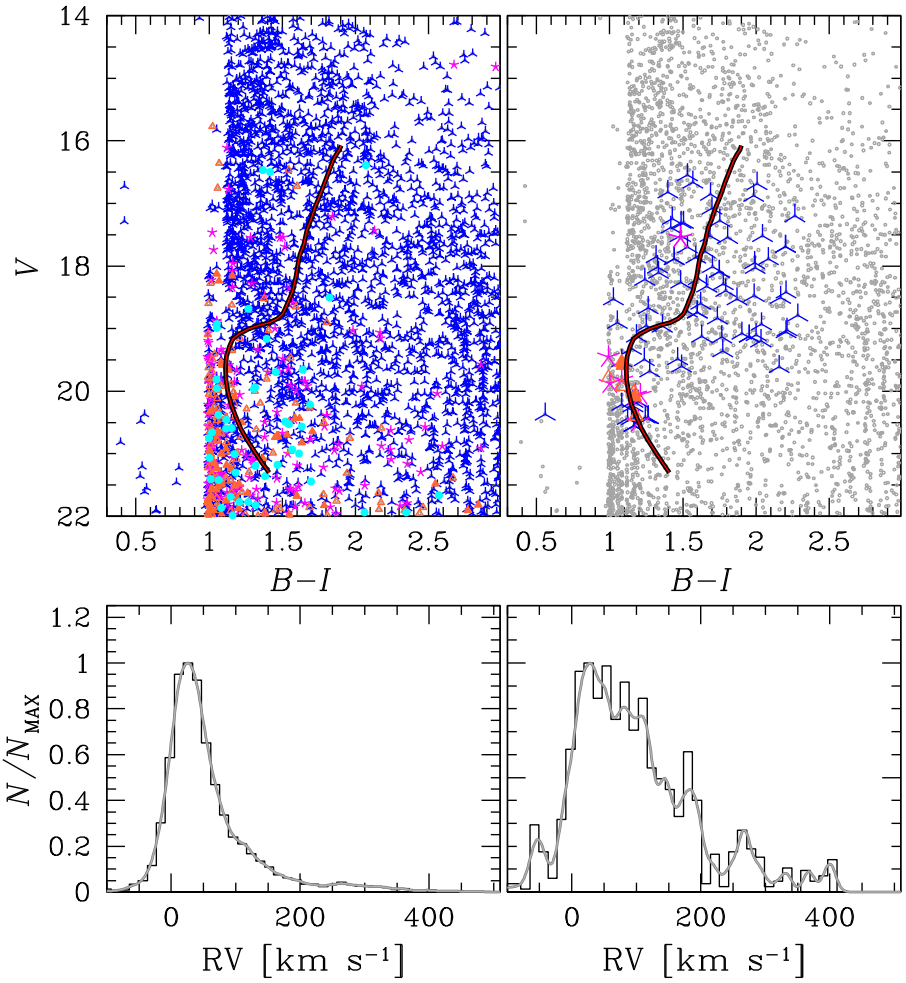

Figure 4. Left-hand panels: V versus $(B - I)$ CMD predicted by the Galactic model by Robin et al. (2003) for all the stars in a 60 arcmin × 60 arcmin field of view centred at the same coordinates as the field studied in this paper (top). We used the same symbols introduced in Fig. 3 to represent stars in different RV intervals. The histogram and the kernel-density distribution of RVs predicted by the Galactic model for the same stars are shown in the lower-left panel. Right-hand panels: in grey we represent the same CMD as in the upper-left panel; stars that have V and $(B - I)$ similar to the observed stars, belonging to the 'equivalent sample' (see Section 3.1 for details), have been represented according to symbols and colours corresponding to their RV (see Fig. 3).

(i) We have defined in the V versus $(B - I)$ CMD a grid of points spaced in colour and in magnitude by $\Delta(B - I) = 0.025$ mag and $\Delta V = 0.05$ mag, respectively.

(ii) We started from the analysis of the observed CMD. For each grid point (i,j) and each observed star (l), we have estimated the probability $(P^l_{\mathrm{OBS},i,j})$ of having that star in a box within $\Delta(B - I)/2$ and ΔV from the point i,j. This probability has been estimated by assuming for each star the errors in colour and magnitude estimated for real stars. For each grid point, we have determined $P_{\mathrm{OBS},i,j} = \sum_{l=1}^{N} P^l_{i,j}$.

(iii) Then, we have generated the equivalent sample by assuming a given value of k, and determined for these stars $P_{k,i,j}$ by following the same procedure as described above for observed stars. The assumed values of k range from $k = 0$ to 10 in steps of 0.1.

(iv) For each value of k, we calculated $\chi(k) = \sum(P_{k,i,j} - P_{\mathrm{OBS},i,j})$. The k value that, for our data set, returns the minimum χ is $k = 2.2$.

For the determination of the equivalent sample, we then assume $k = 2.2$; however, we have verified that the conclusions of our paper are identical for any $1 < k < 10$.

In the upper-right CMD of Fig. 4, we highlight only the selected sample of stars while the rest of the stars is represented with small grey dots. To avoid that our conclusions are affected by low numbers, we have increased the number of selected stars by a factor of 100. To do this, we have generated other 99 Galactic models for stars from Robin et al. (2003) in a 60 arcmin × 60 arcmin region with the same coordinates as the external field of NGC 1851. For each of them, we have extracted a sample of stars as described above. In the following, we use the whole collection of the 100 samples of stars (hereafter 'equivalent sample').

The corresponding RV distribution for these stars in the equivalent sample is shown in the lower-right panel. We conclude that when the velocities of all the stars from the Galactic model are analysed, the distribution has a single peak at RV = 25 km s^{-1} and about 82 per cent of stars have RV < 100 km s^{-1} (lower-left panel); in the case of the equivalent sample (lower-right panel), the main peak is shifted to higher velocities, at RV ∼ 50 km s^{-1}, and the fraction of stars with RV < 100 km s^{-1} decreases to ∼65 per cent. There is some hint of less prominent peaks at RV ≈ 100, ≈180 and ≈270 km s^{-1}.

A comparison between the RV distribution determined in this paper and that expected from the Galactic model is provided in the

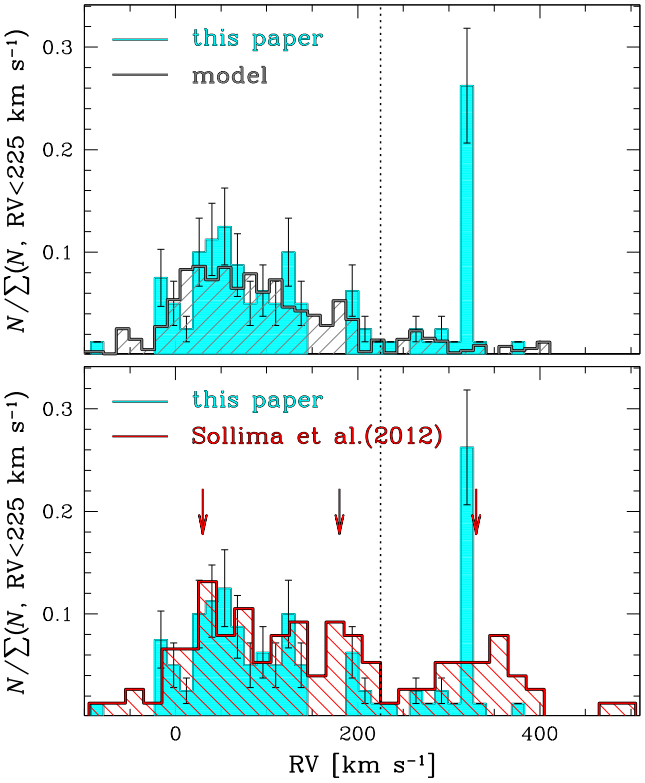

Figure 5. Upper panel: comparison of the RV distribution observed in this paper for the halo of NGC 1851 (cyan histogram) and the distribution predicted by the Galactic model by Robin et al. (2003, grey-dashed histograms). Lower panel: comparison between the RV distribution derived for the halo in this paper (cyan) and by S12 (red-dashed). The red arrows indicate the three peaks found in S12, attributed to the field, a possible stream and the halo associated with NGC 1851.

upper panel of Fig. 5. To properly compare the two distributions, we have normalized each histogram to the total number of stars with RV < 225 km s^{-1}, which is the value marked by the vertical dotted line of Fig. 5. By considering all our analysed stars, the probability that the observed RVs and those from the model come from the same parent distribution is almost null ($P < 10^{-5}$), not depending on the adopted normalization. The most striking difference between the two distributions is the lack of stars with $310 <$ RV < 340 km s^{-1} in the model. Indeed while 23 stars have been observed in this interval of RV, the Besançon model predicts that only ∼1.5 stars have such kinematics. This provides further support of a halo of stars, with the same kinematic as NGC 1851 but located between 1 and ∼2.5 tidal radii from the cluster centre. If we neglect these stars and consider only stars with RV < 300 km s^{-1}, the observed and expected RV distributions are very similar as confirmed by the Kolmogorov–Smirnov (KS) test which provides a probability $P = 0.85$ to come from the same parent distribution. Regarding the small contamination from field stars that can occur at the RV of NGC 1851 (<2 stars, as suggested from the models), we note that 2 out of the 23 stars (T066 and T073) in our sample of NGC 1851 RV-like halo stars do not lie on the fiducial sequence of the cluster. The chemical abundance analysis for these two stars has been inferred in a similar way as the other halo stars. However, keeping in mind that we cannot exclude that these objects are field stars, when necessary, we will highlight the presence of these two stars along the paper.

3.2 Comparison with Sollima et al. (2012)

The first RV study of stars in the halo of NGC 1851 was conducted by Sollima et al. (2012, hereafter S12) based on VIsible Multi-Object Spectrograph/Very Large Telescope spectra. The 107 stars analysed by S12 are between 12 and 33 arcmin north-east from the centre of NGC 1851; so, even if at a similar distance from the centre of the cluster, the field analysed by S12 observed a different quadrant, and none of their targets is in common with our sample.

In the lower panel of Fig. 5, we compare the RV histogram distributions from this paper (cyan) and from S12 (red), obtained by binning in intervals of 20 km s^{-1}. Both histograms are normalized to the total number of stars with RV < 225 km s^{-1} (vertical dotted line of Fig. 5). We emphasize that caution must be used when comparing the two RV distributions as the stars studied by S12 and those analysed in this paper have not been selected homogeneously.

S12 identified three main peaks in their RV distribution. They associated most of their stars to foreground disc stars peaked around RV ~ 30 km s^{-1}, and then they found a peak at RV ~ 330 km s^{-1} corresponding to the bulk motion of NGC 1851 and an overdensity of stars at RV ~ 180 km s^{-1}. The position of the three peaks inferred by S12 is highlighted in the lower panel of Fig. 5 by red arrows. The comparison of the two observed distributions shows that the uncertainties associated with the RV measurements are much higher in S12, due to the lower resolution data they used. Their estimated internal uncertainty, of ∼15 km s^{-1} (see S12 for details), reflects in a much broader distribution of stars about the peak at the RV of NGC 1851. On the basis of their RV distribution, S12 suggested that, apart the bulk of stars at the same mean RV of the cluster, the overdensity at ∼180 km s^{-1} could be associated with a cold stream having $\sigma_{RV} < 20$ km s^{-1}. However, they pointed out that additional studies are needed to confirm this possibility.

Our RV distribution exhibits a sharp peak at the same motion as NGC 1851, and a broad peak around RV ≈ 50 km s^{-1} in close analogy with that observed by S12. Our RV distribution does not show any peak of stars at RV ≈ 180 km s^{-1}, but we observed two small groups of stars at the similar velocities of RV ≈ 110 and $\approx$200 km s^{-1}. We recall here that the RV distribution observed from the data set analysed in this paper for stars with RV < 300 km s^{-1} is fully consistent with that predicted by the Galactic model by Robin et al. (2003), which also predicts a minor peak at RV ~ 180 km s^{-1}, thus excluding any evidence of a stellar stream associated with NGC 1851 in our field of view.

4 CHEMICAL ABUNDANCE ANALYSIS

Our sample is almost entirely composed of low-luminosity dwarfs and subgiants. In fact, during the target selection we wanted to maximize the number of possible NGC 1851 halo stars, with stars as close as possible to the cluster sequences along the CMD. As the RGB is relatively poorly populated, we selected mostly MS stars. In the end, our sample was successful in the identification of 23 stars belonging to the NGC 1851 halo. Among the 23 stars with NGC 1851-like RVs, we were able to estimate metallicities for 15 objects, including 7 stars with both Sr and Ba estimates, thus providing the first elemental abundances for the halo surrounding NGC 1851; the other stars had insufficient S/N.

The chemical abundances that we were able to estimate for the halo stars were then compared with those obtained for the central field of NGC 1851. To have all the measurements in the same absolute scale, we have analysed both the external and the internal field in a uniform manner (e.g. same code and linelist).

Table 3. Adopted atmospheric parameters and chemical abundances for the NGC 1851 halo and cluster (central field) stars. When available, we list the scatter derived from individual measurements. The full versions will be available online as supplementary material.

ID	$T_{\rm eff}$	$\rm err_{Teff}$	log g	$\xi_{\rm t}$	[Fe/H]	σ	[C/Fe]	[Mg/Fe]	Scatter	[Ca/Fe]	[Cr/Fe]	[Sr/Fe]	Scatter	[Ba/Fe]
							Halo							
T198	5296	59	3.55	1.02	−1.36	0.04	−0.27	0.53	0.3	0.43	−0.25	−0.06	0.23	0.27
T132	5966	107	4.29	1.11	−1.29	0.09	–	–	–	0.37	–	0.33	–	–
T150	5857	89	4.31	1.07	−1.34	0.07	–	–	–	–	–	–	–	0.75
							Cluster							
SGB-a.10	5923	1389	3.90	1.15	−1.05	0.06	−0.47	0.31	0.11	−0.02	−0.25	−0.26	0.01	0.40
SGB-a.12	5793	89	3.84	1.11	−1.25	0.11	−0.32	–	–	–	−0.49	−0.32	–	0.54
SGB-a.13	5716	81	3.78	1.10	−1.48	0.04	−0.03	0.58	–	0.19	0.13	0.17	0.02	0.28

4.1 Model atmospheres

As the moderate resolution and wavelength range of our spectra do not allow us to determine atmospheric parameters from Fe lines, we used our photometry to estimate effective temperatures ($T_{\rm eff}$) and surface gravity (log g) of our stars. Photometry includes *BVRI* for the inner field and *BVI* for the halo field. The photometry is adjusted by assuming a reddening value, in this case $E(B-V) = 0.02$, and then computing an extinction for each bandpass using the Cardelli, Clayton & Mathis (1989) extinction curve and adopting $R_V = 3.1$. The reddening is assumed constant across the field, which should be reasonable for such a low-reddening system, and the results are only weakly dependent on variations in $E(B-V)$ of 0.01.

Effective temperatures and their uncertainties are estimated via Markov chain Monte Carlo (MCMC) simulations using the parallel EMCEE package (Foreman-Mackey 2010). The EMCEE code takes as input model parameters and a probability function that compares models to individual data points. The log-probability function is the sum of the squares of the differences between observed and modelled magnitudes, divided by the error, in each filter.

The modelled magnitudes are obtained by interpolating within grids of bolometric corrections for all photometric bands (*BVRI* for the inner field, *BVI* for the outer field) and assuming that all cluster stars are equidistant. Essentially we construct an Hertzsprung-Russell (H-R) diagram from the input CMD, and map a given star to the point on the H-R diagram that best matches the observed photometry. The bolometric corrections are derived from PHOENIX model atmospheres (Hauschildt, Allard & Baron 1999a; Hauschildt et al. 1999b) using the *BVRI* bandpasses defined by Bessell & Murphy (2012). These calculations assume [Fe/H] $= -1.3$ and [α/Fe] $= +0.2$ broadly consistent with the finding reported in this paper. However, it is important to note that the effective temperatures derived in this way have only weak sensitivity to [Fe/H] because of the broad-band, optical nature of the photometry.

The MCMC simulations provide estimates of effective temperature, bolometric luminosity and surface gravity. The surface gravity is very roughly determined because of its weak dependence on broad-band photometry. The resulting estimate of $T_{\rm eff}$ for a given star is obtained from the Markov chain, which samples the posterior probability density function, by computing the mean and standard deviation. A star with a large standard deviation also tends to have a mean that differs considerably from the median, suggesting that the distribution is asymmetric. However, such stars are rare in the present data set (<10 per cent in both fields).

Surface gravities are obtained from the apparent V magnitudes, corrected for differential reddening, the $T_{\rm eff}$, apparent bolometric luminosities obtained from the MCMC simulations above and an apparent distance modulus of $(m-M)_V = 15.47$ (Harris 1996, 2010 edition). We assume that all stars lie at essentially the same distance and masses resulting from one single best-fitting isochrone.[4] For microturbulent velocities ($\xi_{\rm t}$), we adopted the latest version of the appropriate relation used in the *Gaia*-ESO survey (GES, Gilmore et al. 2012; Bergemann et al., in preparation), assuming a metallicity of [Fe/H] $= -1.18$ dex for NGC 1851. The dispersion of the recommended $\xi_{\rm t}$ values for the GES UVES spectra around the adopted relation is about 0.20 km s^{-1}, which is a reasonable internal uncertainty to be associated with our adopted values.

We note that our technique to derive effective temperatures is independent of the projection of stars on any isochrone, as there is no isochrone used in the MCMC process. The model dependence of our technique is related to the different set of colours used (e.g. Castelli & Kurucz or MARCS instead of PHOENIX), and to the fact that we used a fixed metallicity and distance. On the other hand, our $T_{\rm eff}$ values do not depend on projecting on isochrone projection.

If projecting on theoretical sequences has the advantage to minimize the impact of photometric errors on the derived atmospheric parameters, on the other hand in GCs like NGC 1851 with multiple SGB and RGB sequences, one single isochrone is not able to represent all the observed populations. We prefer to use the actual photometric data for each star, instead of using multiple isochrones, to not force each star to a given isochrone; this allows us to avoid errors due to mismatch between the observed stars and the two SGBs, which may occur due to photometric errors, and in regions of the CMD (like the upper MS) where it is not possible to assign the observed stars to different populations just on photometric information. Furthermore, we do not want to impose a *two discrete SGBs* scenario, as we cannot exclude that the real situation may be more complex.

Table 3 lists the adopted stellar parameters for the NGC 1851-like RV stars in the halo and the central field stars. The uncertainties on the $T_{\rm eff}$ values given by the MCMC simulations are listed in the third column of Table 3. The median of these errors is 94 ± 2 K (rms = 17 K), and we adopt this value as an estimate of the internal error associated with our $T_{\rm eff}$.

An independent temperature estimate was obtained from the Hδ line index (HP2), calibrated as a function of $T_{\rm eff}$ (Ryan, Norris & Beers 1999), and the quadratic relationship provided in Norris et al. (2013) obtained for metal-poor dwarfs, subgiants and giants. The adopted $T_{\rm eff}$ as a function of the values derived from the HP index

[4] We note that the masses on the two SGB populations of NGC 1851 may be different, but, at a given magnitude, this difference is of the order of ∼0.01 $M_\odot$. A possible systematic error in the adopted masses of that order has negligible effects (<0.01 dex) on the log g values and on the derived abundance.

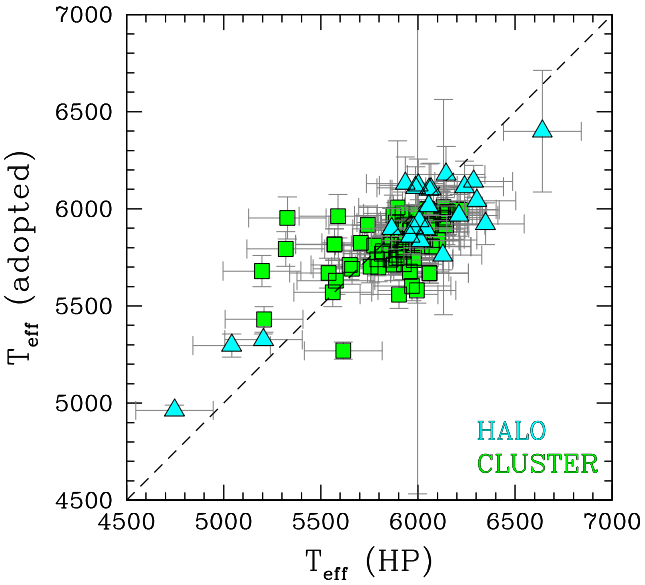

Figure 6. Adopted $T_{\rm eff}$ values for the NGC 1851 halo (cyan triangles) and central field (green squares) targets as a function of the values obtained from the HP index.

has been shown in Fig. 6 for the NGC 1851 halo and NGC 1851 central field stars. The halo and cluster stars' adopted $T_{\rm eff}$ values compare similarly to those obtained from the HP index, with mean differences $\Delta T_{\rm eff}$(HP−adopted) = 55 ± 39 K (rms = 184 K) for the NGC 1851 halo and $\Delta T_{\rm eff}$(HP−adopted) = 73 ± 21 K (rms = 191 K) for the central field stars. This comparison confirms that the temperature scale adopted for the NGC 1851 halo stars agrees with the one adopted for the NGC 1851 cluster stars.

Errors in $T_{\rm eff}$ and mass of ± 94 K and ± 0.05 $M_\odot$ affect the log g values by ± 0.03 and ± 0.02 dex, respectively. Internal uncertainties in the bolometric luminosity of ± 0.01 have small effects on log g values: ∓0.01 dex. All these effects, added in quadrature, contribute to a very small internal error in log g of ≈0.04 dex. We emphasize that this is just the formal internal error in log g while real uncertainties in this parameter may be much larger. Internal uncertainties of ± 94 K and ± 0.04 dex in $T_{\rm eff}$ and log g affect $\xi_{\rm t}$ by only ± 0.03 km s^{-1}. Although the internal error in $\xi_{\rm t}$ due to $T_{\rm eff}$ and log g is formally small, we assume for this parameter a more realistic internal error that is the rms of the GES UVES data around the used relation, i.e. we used an error of ∼0.20 km s^{-1}. We will take into account these uncertainties in the atmospheric parameters for the estimation of the errors associated with the chemical abundances.

In Fig. 7, we compare the adopted atmospheric parameters with those of G12 for the central field of NGC 1851. Effective temperatures and surface gravities from G12 have been determined by fitting two different isochrones for stars associated with the bright SGB (bSGB) and fSGB of NGC 1851, using different photometric catalogues from those used here (see G12 for details). We note a systematic difference in $T_{\rm eff}$ with the G12 values being ∼200 K hotter, with a scatter of 59 K. Only three stars of the internal field are in common with Lardo et al. (2012), whose $T_{\rm eff}$ have been determined from the Alonso calibrations (Alonso, Arribas & Martínez-Roger 1999). For two of these stars, our $T_{\rm eff}$ are higher by ∼300 K and one is slightly lower (by 40 K). These comparisons suggest that, although the $T_{\rm eff}$ scale may be affected by systematics of a few hundreds of K, the internal error is lower (∼100 K). The mean difference in log g between the G12 and the adopted values is small, of 0.04 dex (rms = 0.02 dex). Microturbulent velocities in G12 are lower by 0.17 km s^{-1} (rms = 0.06 km s^{-1}). The different $\xi_{\rm t}$ values (as appear in Fig. 7) are likely due to the different relations used to estimate this parameter. While our relation is a second-order polynomial in $T_{\rm eff}$, log g and metallicity, G12 used a linear relation in just the surface gravity.

4.2 Abundance analysis

Chemical abundances were derived from a local thermodynamic equilibrium (LTE) analysis by using the latest version of the spectral analysis code MOOG, with no scattering included (Sneden 1973), by using the α-enhanced model atmospheres of Castelli & Kurucz (2004), whose parameters have been obtained as described in Section 4.1. All the target lines have been analysed by spectral synthesis, via an automatic χ^2-minimization between the synthetic and the observed spectra reported to the same reference continuum.

We determined abundances for Fe, the neutron-capture (*n*-capture) elements Sr and Ba, the light element C, the α elements Mg and Ca, and the iron-peak Cr. Iron abundances were derived from the Fe I spectral features at 4005.2, 4045.8, 4063.6, 4071.7, 4132.1, 4143.9, 4187.0, 4202.0, 4250.1, 4260.5, 4271.2, 4383.6, 4404.8, 4415.1, 4476.0, 4482.2, 4528.6, 4556.1 Å. For the NGC 1851 cluster stars, the S/N of the spectra was sufficient to allow us to synthesize all the Fe features. In the case of the NGC 1851 halo stars, it was possible to infer abundances from all the lines only in the two RGBs. For the other stars, we measured a subsample of the listed Fe features, typically a number of 7–10 spectral features. For

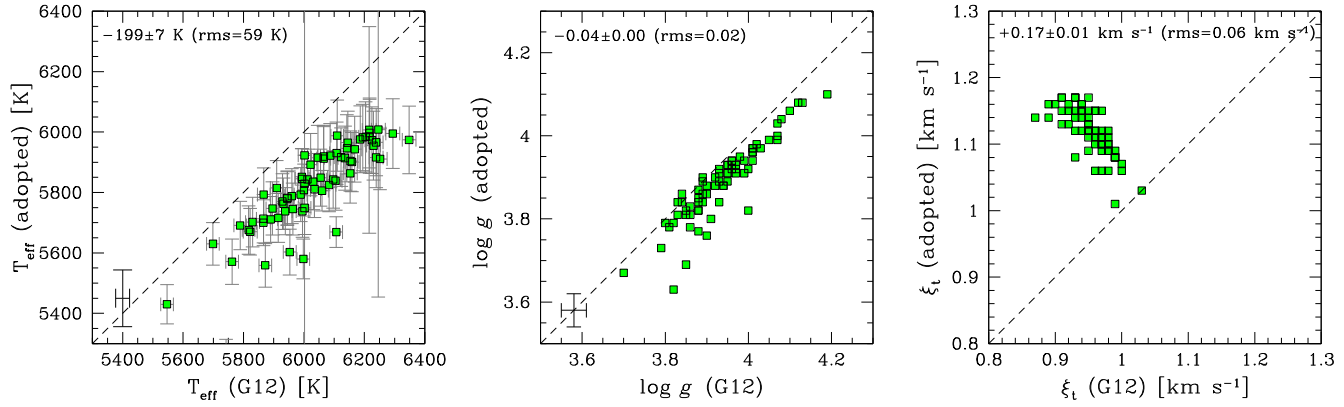

Figure 7. Adopted values for $T_{\rm eff}$, log g and $\xi_{\rm t}$ for the NGC 1851 central field targets as a function of the values adopted in G12. The mean differences (adopted−G12) and associated rms are shown in each panel.

four stars (T128, T153, T134, T139), we could measure only two to three Fe features. To ensure that the derived average metallicities were on the same scale, and avoid systematics depending on the analysed spectral feature for different stars, we corrected the abundances from each measured line for their systematic difference with the abundance obtained from the Fe I 4404.5 Å feature, which is measured in all the stars.

Limited by the relatively low resolution and the small wavelength range of our spectra, we derived Sr and Ba abundances only from the strong resonance transitions Sr II 4077, 4215 Å and Ba II 4554 Å. Both the Sr lines suffer from blends with other surrounding transitions, mostly Fe features and other *n*-capture species (e.g. Dy and La) in the case of the Sr II 4077 Å. For all the contaminating elements, we assumed a solar-scaled abundance. In the case of Sr, the blending with Dy and La transitions occurs on the redward and blueward spectral region around the Sr II 4077 Å line, respectively. The effect of these blending features has been considered by performing spectral synthesis for a few representative stars by varying Dy and La abundances relative to Fe. In both cases, the effect on the [Sr/Fe] abundances is quite small: [Sr/Fe] decreases by less than 0.05 dex by increasing the abundances for these two contaminating elements by +0.5 dex. This variation should be regarded as a possible systematic error affecting mostly the stars in our sample that have been enriched in *n*-capture elements and have super-solar abundances relative to Fe for these elements. We can argue that, in the case of NGC 1851, the Dy contamination may have a negligible effect on the star-to-star relative abundances. This is because in the Solar system Dy is expected to be mostly sensitive to *r*-process nucleosynthesis (87.9 per cent from *r*-processes and 12.1 per cent from *s*-processes; see table 10 in Simmerer et al. 2004). If some stellar populations in NGC 1851 have undergone a substantial enrichment in *s*-processes, we may expect a lower degree of chemical variations, if any, in Dy.

Spectral synthesis in the analysis of our spectral lines (and particularly at our moderate resolution) is needed to take these blends into account. Although the Ba II 4554 Å is isolated from contaminating transitions, we also computed synthesis for the Ba spectral line, to take its isotopic splitting into account.

The linelists are based on the Kurucz line compendium, except the Ba transition for which we added hyperfine structure and isotopic data from Gallagher et al. (2010). For Sr our linelists neglect hyperfine/isotopic splitting since the wavelength shifts are very small and Sr has one dominant isotope.

Barium has five major naturally occurring isotopes whose production fractions in the rapid-process (*r*-process) and *s*-process are significantly different (e.g. Kappeler, Beer & Wisshak 1989). In particular, abundances derived from the Ba II 4554 Å transition are very sensitive to the adopted r/s ratio (e.g. Mashonkina & Zhao 2006; Collet, Asplund & Nissen 2009). In our previous analysis of M22 SGB stars, we found that assuming a pure *r*-process isotopic ratio (Arlandini et al. 1999), instead of a scaled solar-system Ba abundance and isotopic fractions (Lodders 2003), has the effect of decreasing the [Ba/Fe] abundances by ≈0.2 dex (Marino et al. 2012a). Bearing in mind that this behaviour can be an issue in the analysis of NGC 1851 that hosts stars with different contributions from the *s*-process material, we decide to assume scaled-solar system Ba isotopic fractions for all the stars. However, we note that stars with lower Sr and Ba abundances may be better reproduced by an *r*-process isotopic ratio and their Ba abundances may be overestimated in our analysis.

Carbon was measured from spectral synthesis of the CH ($A^2\Delta - X^2\Pi$) *G*-band heads near 4315 Å assuming a solar-scaled oxygen abundance. The molecular line data employed for CH were provided by Plez (private communication; some basic details of the linelist are given in Hill et al. 2002). Given that we do not have information on the actual oxygen abundance of our stars, the assumption of solar-scaled oxygen is reasonable as the [O/Fe] distribution in RGB stars in NGC 1851 spans a range that goes from [O/Fe]∼−0.50 dex to [O/Fe]∼+0.50 dex (Carretta et al. 2010; Villanova et al. 2010). The molecular equilibrium in stellar atmospheres generally affects the abundance of C, N, O. However, in our range of atmospheric parameters CO is not an abundant molecule, and the impact of [O/Fe] abundances varied by the entire range observed in giants (from −0.50 to +0.50 dex) is negligible on the *G* band. Magnesium has been derived from the Mg I lines at ∼4057.5 and 4167.3 Å, calcium from the Ca I at ∼4226.7 Å and chromium from the Cr I line at ∼4254.3 Å.

An internal error analysis was accomplished by varying the temperature, gravity, metallicity and microturbulence one by one, and re-determining the abundances for three NGC 1851 halo stars and three NGC 1851 cluster stars spanning the observed range in temperature. The parameters were varied by $\Delta T_{\rm eff} = \pm$ 100 K, $\Delta \log g$ = 0.05 dex, Δ[Fe/H] = ± 0.11 dex and $\Delta\xi_{\rm t} = \pm$ 0.2 km s^{-1}.

The limited S/N of our spectra introduces significative internal uncertainties to our chemical abundances. To estimate these uncertainties, we computed a set of 100 synthetic spectra for three inner field stars (SGB-a.9, SGB-a-St.24 and SGB-b-St.21) and two halo stars (T186 and T198), whose atmospheric parameters are representative of the whole sample. These set of synthetic spectra were calculated by using the best-fitting inferred abundances, and were then degraded to the S/N of the observed spectra. We then analysed the chemical abundances of all these synthetic spectra in the same manner as the observed spectra. The scatter that we obtain from the abundances from each spectral line for a set of synthetic spectra corresponding to a given star represents a fair estimate of the uncertainty introduced by the fitting procedure, due to the S/N, the pixel size and the continuum estimate. These uncertainties strongly depend on the S/N and are higher for halo stars with lower S/N. The mean errors in the chemical abundances from our fitting procedure are then divided by the square root of the number of available spectral lines to obtain an estimate of the uncertainty associated with each analysed element. These errors are listed as $\sigma_{\rm fit}$ in Table 4. Since these errors are random, the uncertainty is lower for those elements with a large number of lines (e.g. Fe). For the other elements, we have two (or just one) lines, and this error contribution is higher. Of course, the larger uncertainties are found for the MS stars of the halo that have a lower S/N.

A list of the uncertainties in chemical abundances due to the various considered sources is provided in Table 4, where double entries in the errors for the halo stars mean that the estimated error is different for RGB and MS stars. The various errors were added in quadrature, resulting in typical uncertainties of ∼0.10–0.20 dex,[5] with Ba abundances having the largest uncertainty of $\gtrsim$0.20 dex, which stems mostly from uncertainties in log *g*, $\xi_{\rm t}$ and the limited S/N. Iron abundances over hydrogen are mostly affected by uncertainties in $T_{\rm eff}$, while the limited S/N translating into continuum errors gives the major contribution to the other species.

[5] The fact that an error in the atmospheric parameters can affect in a different way a given element can generate spurious correlations between abundance ratios. As an example we verified through Monte Carlo simulations that we expect a significant correlation between [Fe/H] and [Ca/Fe] due to the errors listed in Table 4.

Table 4. Sensitivity of derived abundances to the atmospheric parameters and the fitting procedure. We reported the total formal error ($\sigma_{\rm total}$) due to the atmospheric parameters plus errors in the fitting procedure ($\sigma_{\rm fit}$).

	$\Delta T_{\rm eff}$ ($\pm$ 100 K)	$\Delta\log g$ ($\pm$ 0.05)	$\Delta\xi_{\rm t}$ ($\pm$ 0.20 km s^{-1})	Δ[A/H] ($\pm$ 0.11 dex)	$\sigma_{\rm fit}$	$\sigma_{\rm total}$
			Halo			
[C/Fe]	$\pm$ 0.04	$\pm$ 0.01	$\pm$ 0.02	$\mp$0.02	$\pm$ 0.10/ $\pm$ 0.16	0.11/0.17
[Mg/Fe]	$\mp$0.08	$\mp$0.01	$\pm$ 0.01	$\pm$ 0.01	$\pm$ 0.13/ $\pm$ 0.18	0.15/0.20
[Ca/Fe]	$\pm$ 0.03	$\pm$ 0.00	$\pm$ 0.02	$\mp$0.02	$\pm$ 0.09/ $\pm$ 0.13	0.10/0.14
[Cr/Fe]	$\pm$ 0.17	$\mp$0.01	$\mp$0.02	$\mp$0.02	$\pm$ 0.18/ $\pm$ 0.38	0.25/0.42
[Fe/H]	$\pm$ 0.10	$\mp$0.02	$\mp$0.02	$\mp$0.10/$\mp$0.07	$\pm$ 0.02/ $\pm$ 0.07	0.15/0.14
[Sr/Fe]	$\mp$0.01	$\pm$ 0.02	$\mp$0.02	$\pm$ 0.02	$\pm$ 0.12/ $\pm$ 0.20	0.13/0.20
[Ba/Fe]	$\mp$0.07/$\mp$0.04	$\mp$0.11	$\mp$0.15	$\pm$ 0.02	$\pm$ 0.09/ $\pm$ 0.21	0.22/0.29
			Cluster			
[C/Fe]	$\pm$ 0.04	$\pm$ 0.01	$\pm$ 0.03	$\mp$0.02	$\pm$ 0.06	0.08
[Mg/Fe]	$\mp$0.08	$\mp$0.01	$\pm$ 0.00	$\mp$0.03	$\pm$ 0.13	0.16
[Ca/Fe]	$\pm$ 0.04	$\mp$0.01	$\pm$ 0.02	$\mp$0.02	$\pm$ 0.08	0.09
[Cr/Fe]	$\pm$ 0.06	$\pm$ 0.00	$\mp$0.01	$\mp$0.05	$\pm$ 0.19	0.21
[Fe/H]	$\pm$ 0.10	$\mp$0.01	$\mp$0.03	$\mp$0.07	$\pm$ 0.03	0.13
[Sr/Fe]	$\mp$0.04	$\pm$ 0.02	$\pm$ 0.01	$\pm$ 0.04	$\pm$ 0.07	0.09
[Ba/Fe]	$\mp$0.03	$\mp$0.11	$\mp$0.17	$\pm$ 0.00	$\pm$ 0.11	0.23

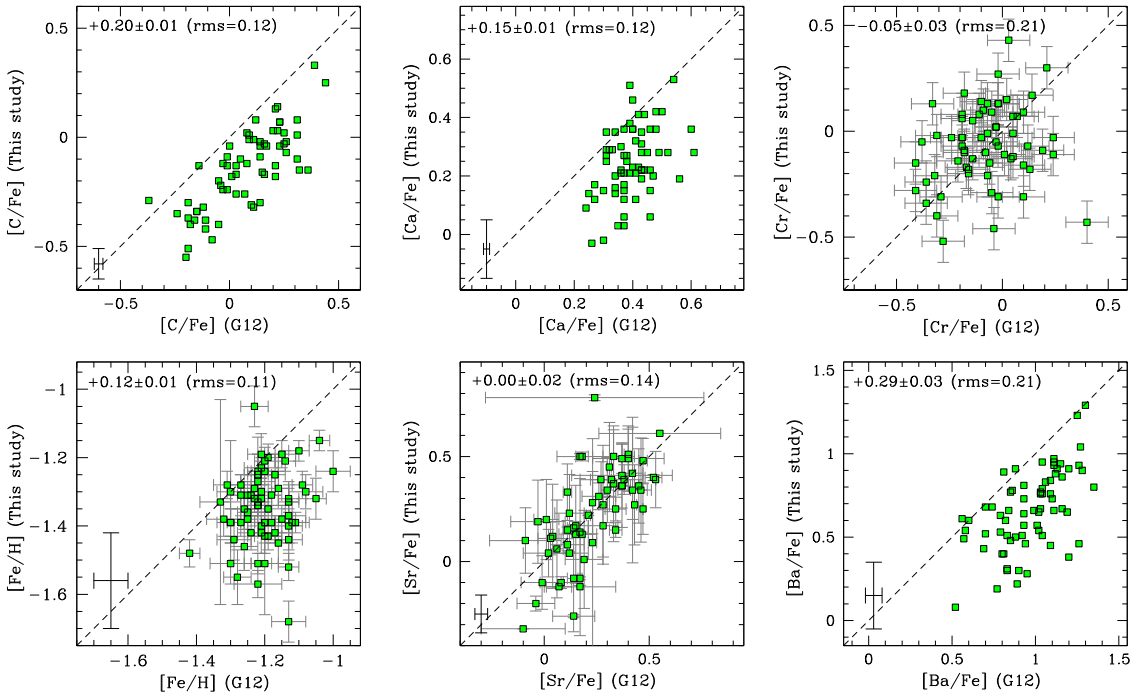

Figure 8. Chemical abundances inferred in this study for the NGC 1851 central field targets as a function of those from G12. The mean differences (G12−adopted) and associated rms are shown in each panel.

A comparison of our chemical contents inferred for the central field with those from G12 is shown in Fig. 8, for those species analysed both in this study and in G12. This comparison reveals some systematics between our abundances and theirs, the most of which can be explained by the systematic differences in the adopted atmospheric parameters discussed in Section 4.1. As an example the difference in [Fe/H] of ∼0.20 dex can be entirely ascribed to the systematically higher $T_{\rm eff}$ values in G12, while the large systematics in [Ba/Fe] of ∼0.30 dex are mostly due to our higher $\xi_{\rm t}$ and, in minor part, to our slightly lower log g. We note that the systematic effects on stellar parameters seem to cancel each other in the cases of [Cr/Fe] and [Sr/Fe]; the systematics observed in [C/Fe] and [Ca/Fe] cannot be explained by differences in the atmospheric parameters, and may instead be due to different linelists and/or to possible systematics in the continuum placement.

The values of the observed rms for those elements with no significant internal variations can be used as a rough estimate of our internal errors, to be compared with the expected ones. In Table 5, we list the 68th percentile of the distributions of the inferred abundances, together with the median values for the NGC 1851 halo stars and the NGC 1851 cluster stars. By comparing the 68th percentile values listed in the third column, with the expected total uncertainties (Table 4), we note that, in general, the errors are in rough agreement. The element that clearly stands out is strontium. We will discuss this point in the next section.

Table 5. Median and 68th percentile (σ_{obs}) of the chemical abundances for the NGC 1851 halo and the cluster total, bSGB and fSGB samples.

	Halo		Cluster		bSGB cluster		fSGB cluster	
	avg.	σ_{obs}	avg.	σ_{obs}	avg.	σ_{obs}	avg.	σ_{obs}
[Fe/H]	-1.35 ± 0.02	0.09	-1.33 ± 0.01	0.09	-1.35 ± 0.01	0.08	-1.30 ± 0.02	0.11
[C/Fe]	-0.27 ± 0.09	0.17	-0.13 ± 0.02	0.18	-0.09 ± 0.02	0.15	-0.24 ± 0.04	0.18
[Mg/Fe]	$+0.51 \pm 0.02$	0.03	$+0.44 \pm 0.02$	0.16	$+0.41 \pm 0.02$	0.15	$+0.54 \pm 0.03$	0.13
[Ca/Fe]	$+0.31 \pm 0.04$	0.10	$+0.25 \pm 0.01$	0.11	$+0.25 \pm 0.02$	0.10	$+0.28 \pm 0.03$	0.13
[Cr/Fe]	-0.09 ± 0.25	0.45	-0.05 ± 0.02	0.18	-0.05 ± 0.03	0.18	-0.05 ± 0.03	0.16
[Sr/Fe]	$+0.10 \pm 0.06$	0.15	$+0.25 \pm 0.03$	0.23	$+0.13 \pm 0.03$	0.21	$+0.39 \pm 0.02$	0.11
[Ba/Fe]	$+0.52 \pm 0.09$	0.28	$+0.66 \pm 0.03$	0.24	$+0.57 \pm 0.03$	0.17	$+0.83 \pm 0.03$	0.16

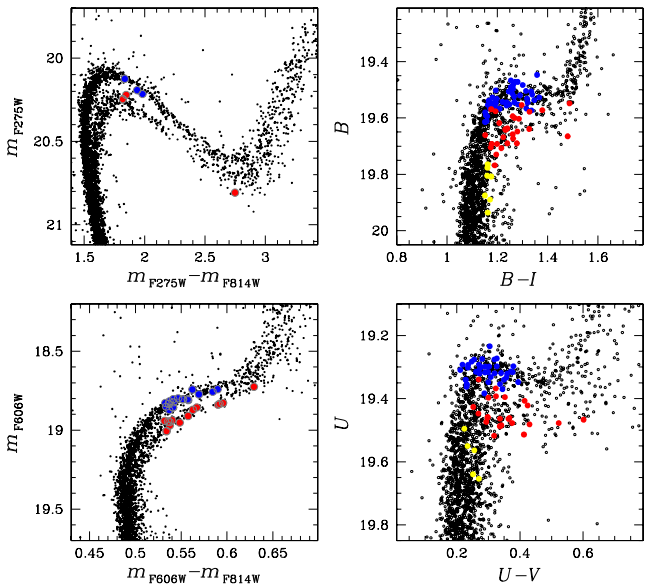

Figure 9. Distribution of the inner field spectroscopic targets on the m_{F275W}–($m_{F275W} - m_{F814W}$) (from Piotto et al. 2012), m_{F606W}–($m_{F606W} - m_{F814W}$) (from Milone et al. 2008), B–($B - I$) and U–($U - V$) CMDs (Milone et al. 2009). Stars assigned to the bSGB and fSGB have been represented in blue and red, respectively; stars with more uncertain location respect to the double SGBs have been coloured in yellow.

5 THE CHEMICAL CONTENT OF THE NGC 1851 SYSTEM

The mean chemical abundances for the NGC 1851 RV-like stars are listed in Table 5, along with those obtained for the central field. In the following, we first discuss results for the NGC 1851 cluster stars in the internal field, so that the chemical composition of the NGC 1851 halo stars can be compared with those of the central cluster.

5.1 The inner field composition

The chemical composition of NGC 1851 is not *standard* for a GC, as it shows internal variations in *s*-process elements, that is a peculiarity of a few GCs such as those showing split SGBs (e.g. M22 and ω Centauri). A proper comparison between the external and internal field of this GC requires accounting for these features.

Starting with the analysis of the cluster stars in the internal field, we have assigned each target to the fSGB or the bSGB, based on their position on the CMD. In Fig. 9, we show the position of these central field targets on the CMD in various photometric bands. An inspection of this figure suggests that the separation between bSGB and fSGB is much more distinct by using ACS and WFC2 images from *HST* (left-hand panels) than by using standard broad-band photometry from ground (right-hand panels). As the photometry from space is more precise, we use the *HST* photometric information to assign each star to the bSGB or the fSGB, when available. In Fig. 9, the bSGB and fSGB spectroscopic targets have been represented in blue and red, respectively. These colour codes will be used consistently in the following discussion. In some cases, the association with one of the two SGBs is not obvious for stars having only ground-based photometry, as some targets lie on the MS where the split is not visible. So, we define a third group of stars whose position on the CMD is ambiguous (yellow dots in Fig. 9), and we do not consider them in the comparison with the halo star chemical composition. In total we have identified 18 bSGBs and 15 fSGBs in the *HST* field, and 32 bSGBs and 14 fSGBs in the ground-based photometry, with 7 uncertain stars.

To properly compare the abundances obtained in the halo with those of the stellar groups observed in the cluster, we derive the average abundances of the bSGB and fSGB samples, as listed in Table 5. In the following discussion, the comparison between the average abundances of the various analysed groups of stars (bSGB, fSGB and halo) has been performed by using as error the quadratic sum of the errors associated with the considered means.

The [Fe/H] histogram of the two SGB groups is shown in the upper panel of Fig. 10. The total distribution of the entire sample, represented in green, is entirely within that expected from the error analysis of our relatively low-resolution data. By dividing the sample into bSGB and fSGB, our mean [Fe/H] values agree within observational errors, suggesting that the two populations have the same average metallicity within ∼0.05 dex ($\Delta_{\text{fSGB-bSGB}} = +0.05 \pm 0.03$), confirming previous studies on the RGB based on higher quality data (Villanova et al. 2010). A smaller difference between the iron content of the two SGBs cannot be ruled out by our data. We recall here that the trends in the [*X*/H] abundances cannot be interpreted in support of any overall metallicity variation as they can result from our observational errors.

The strontium-to-iron ratio, [Sr/Fe], exhibits a large star-to-star variation, exceeding the observational errors. By dividing stars in bSGB and fSGB, the [Sr/Fe] mean abundance of the fSGB is larger than that inferred for the bSGB, with a mean difference $\Delta[\text{Sr/Fe}]_{\text{bSGB-fSGB}} = -0.25 \pm 0.04$ (a $\sim 6\sigma$ significant difference). Despite the large errors on [Ba/Fe], the fSGB is also richer in barium by 0.26 ± 0.04 dex (with a significance of more than 6σ). In summary, our results on the internal field confirm previous findings on the presence of two groups of stars in NGC 1851 with different abundances in those elements mostly produced in the *s*-processes, like Sr and Ba (e.g. Yong & Grundahl 2008; Villanova et al. 2010), and that the fSGB is populated by stars that have undergone some kind of enrichment from these processes (e.g. G12). In this respect,

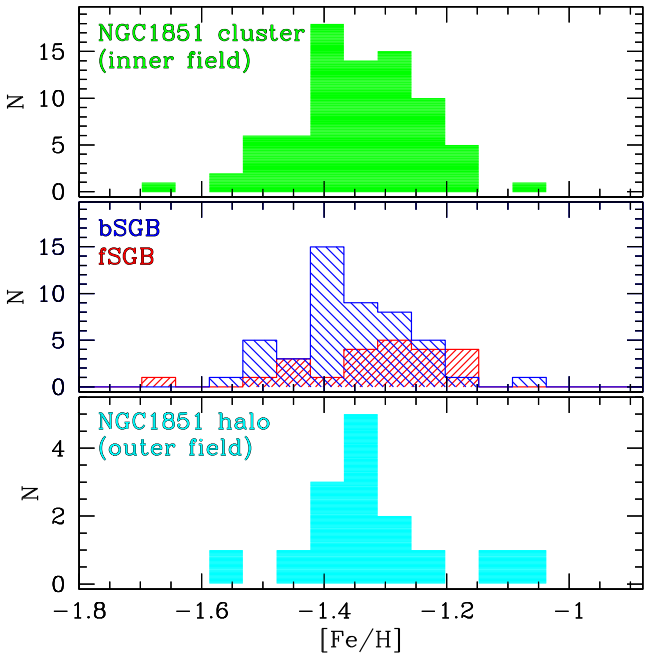

Figure 10. Distribution of the [Fe/H] abundances for the NGC 1851 stars in all the stars in the inner field (upper panel), the bSGB and fSGB (middle panel), and for the NGC 1851 RV-like halo stars (lower panel).

NGC 1851 is very similar to M22, which shows a bimodal distribution in *s*-elements (Marino et al. 2009) and an fSGB populated by stars with higher *s*-element abundances (Marino et al. 2012a).

As a visual representation of the differences in Sr and Ba between the two SGBs, in Fig. 11 we represent some portions of the analysed spectra around key spectral features for one bSGB star (SGB-a-St.45) and one fSGB star (SGB-b-St.16). Superimposed on the observed spectra are the best-fitting synthesis (solid red), two syntheses corresponding to Sr, Ba and Fe abundances varied by ± 0.2 dex and a synthesis computed with the average abundance of the fSGB and the bSGB (dashed red) for SGB-a-St.45 and SGB-b-St.16, respectively.

The high dispersion in [C/Fe], significantly exceeding observational errors, suggests that the abundance in this element shows internal variations. This is consistent with what was observed in other GCs, including the less complex ones (e.g. M4; Marino et al. 2008), and mostly interpreted as due to some kind of intracluster pollution from material that has undergone H-burning at high temperature. It is worth noting here that the high dispersion in [C/Fe] observed in the complete sample does not diminish by dividing stars in bSGB and fSGB, being only marginally lower for the bSGB (Table 5). The average [C/Fe] is higher in the bSGB, with a mean difference of $\Delta([C/Fe])_{bSGB\text{-}fSGB} = 0.15 \pm 0.045$, that is slightly higher than a 3σ level. The chemical pattern of [C/Fe], its variation within different *s*-groups and the larger spread among the *s*-poor (bSGB) stars agree with previous findings obtained first for M22 (Marino et al. 2011a; 2012a) and then for NGC 1851 itself (G12; Lardo et al. 2012).

We note that [Mg/Fe] appears to be slightly higher in fSGB stars (at a level of $\sim 3.5\sigma$). Magnesium abundances for RGB stars in NGC 1851 have been provided by Yong & Grundahl (2008) from UVES spectra and Carretta et al. (2010) from GIRAFFE spectra. The average [Mg/Fe] abundance for their sample of RGB stars is $+0.38 \pm 0.03$ ($\sigma = 0.07$) and $+0.38 \pm 0.01$ ($\sigma = 0.04$) in Yong et al. and Carretta et al., respectively. Although a direct comparison with these two studies cannot be done, because they use different spectral Mg features and possible non-LTE corrections may apply differently. We note that their values are consistent with the average abundance that we found for the total sample of SGB stars, $[Mg/Fe]_{all\,SGB} = +0.44 \pm 0.02$ ($\sigma = 0.16$), and for the bSGB stars, $[Mg/Fe]_{bSGB} = +0.41 \pm 0.02$ ($\sigma = 0.15$). On the other hand, the Mg abundance of the fSGB appears to be higher, but a similar effect has not been found in previous studies on the RGB. Given our large uncertainties associated with individual Mg abundance measurements, the presence of this difference should be viewed with caution and needs to be investigated further. None of the other species appears to show differences among the two SGBs over a 3σ level.

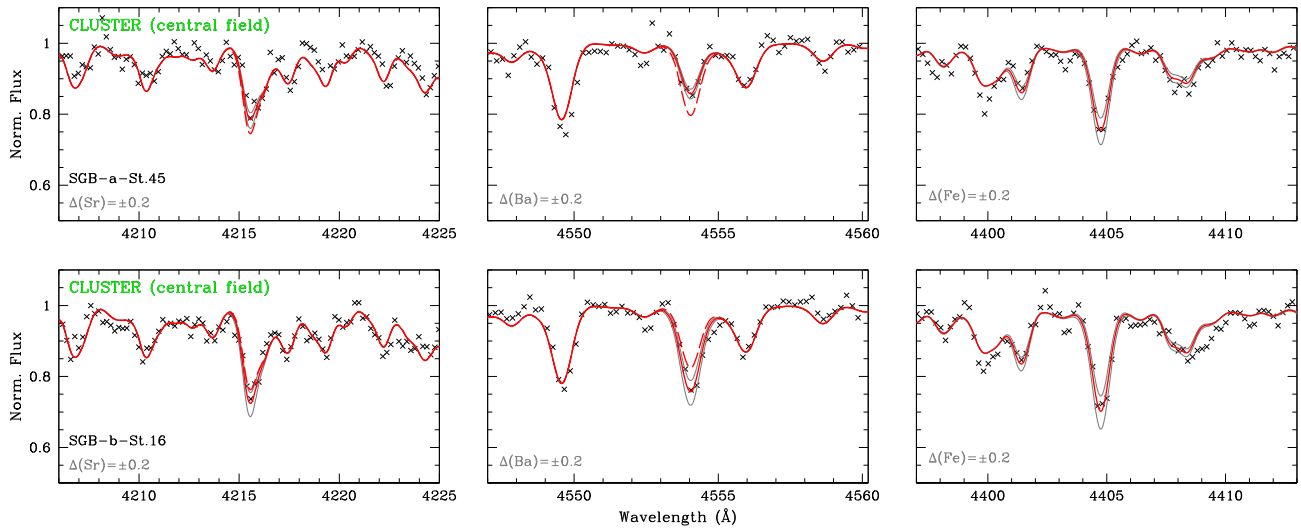

Figure 11. Some examples of observed and synthetic spectra around some measured Fe, Sr and Ba features for two SGB stars in the inner field of NGC 1851. In the upper panel, we plot the spectrum of one bSGB star (SGB-a-St.45), while in the lower panel the spectrum of one fSGB star (SGB-b-St.16). In each panel, the points represent the observed spectrum. The red line is the best-fitting synthesis; to visualize the difference between the mean fSGB and bSGB abundances, we represent with dashed red lines the synthesis corresponding to the average fSGB abundances (upper panel), and to the average bSGB ones (lower panel); the grey lines are the syntheses computed with abundances altered by ± 0.2 dex from the best value.

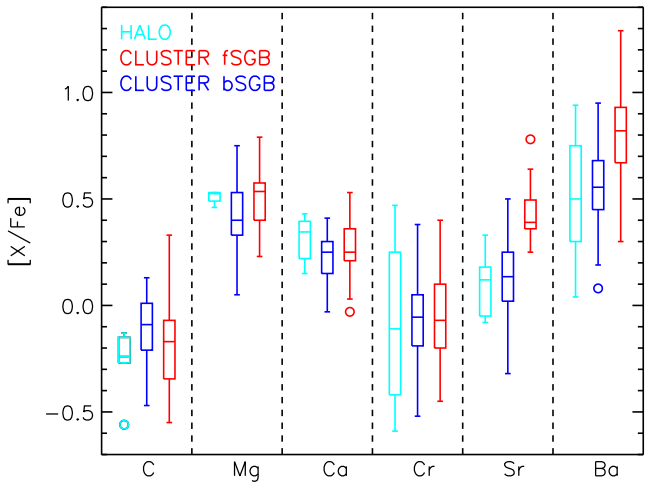

Figure 12. Box and whisker plot of the bSGB (blue), fSGB (red) and halo (cyan) abundances. A boxed horizontal line indicates the interquartile range (the middle 50 per cent of the data) and median found for a particular element. The vertical tails extending from the boxes indicate the total range of abundances determined for each element, excluding outliers. Outliers (those 1.5 times the interquartile range) are denoted by open circles.

5.2 The NGC 1851 halo composition

The chemical abundances and their averages inferred for the halo stars are listed in Tables 3 and 5, respectively. Although we could infer metallicities for a relatively large number of halo stars (15), the abundances of the other elements were possible only in the stars with higher S/N spectra.

The [Fe/H] distribution of the NGC 1851 halo stars is presented in the lower panel of Fig. 10. An inspection of this figure immediately suggests that the distribution for the halo stars spans a range similar to the one observed in the internal field. The average [Fe/H] for the halo stars is [Fe/H] $= -1.35 \pm 0.02$ dex (rms $= 0.09$), and its differences with the mean values obtained for the internal field are Δ[Fe/H]$_{(\mathrm{cluster-halo})} = +0.02 \pm 0.03$ dex, Δ[Fe/H]$_{(\mathrm{bSGBcluster-halo})} = +0.00 \pm 0.03$ dex and Δ[Fe/H]$_{(\mathrm{fSGBcluster-halo})} = +0.05 \pm 0.03$ dex. Indeed, we conclude that, within observational errors, the [Fe/H] in the stars analysed in the halo is consistent with the mean abundance obtained for the NGC 1851 cluster stars.

A comparison between all the abundances inferred for the halo with those obtained for the bSGB and fSGB in the inner field is shown in Fig. 12. The first observation we make is that the [Sr/Fe] distribution for the halo is consistent with that shown by the bSGB, with just one star falling in the range spanned by the fSGB. Although the internal error on [Ba/Fe] is much larger, the [Ba/Fe] range for the halo is also more similar to that spanned by bSGB stars than to that of the fSGB. Note however that, in this case, some stars are also consistent with the fSGB range, but due to the large observational errors affecting barium abundances, we cannot draw strong conclusions on the distribution of this element alone. To quantify the probabilities that the abundance distributions in Sr and Ba obtained for the fSGB, bSGB in the inner field and in those for the outer field derive from the same parent distribution, we performed some KS tests. The KS probability that the bSGB and the fSGB abundances derive from the same distribution is 0.0000 both for Sr and Ba. Similarly low are the probabilities when we compare the fSGB and the halo, for which we obtain 0.0001 and 0.0047 for Sr and Ba, respectively. On the other hand, the probabilities that the bSGB and the halo Sr and Ba abundances derive from the same distribution are 0.8180 and 0.5622, respectively.

In Fig. 13, we show the spectral features for Sr and Ba in three halo stars, with the best-fitting synthesis (blue) and the synthesis corresponding to the mean chemical abundances for the fSGB observed in the inner field (red). This figure illustrates well the limit of our observations: e.g. while the chemical abundances of the two RGBs (T207 and T198) are well distinct from the composition of the fSGB, the uncertainties associated with some MS stars (e.g. T138) are much larger. In the particular case of T138, the star with the most ambiguous position on the [Ba/Fe]–[Sr/Fe] plane (see Fig. 14), the abundances for barium and strontium are in fact only slightly lower than the fSGB average abundance.

Keeping in mind all the uncertainties we have, in particular for the MS stars, the most robust comparison between the halo and the cluster stars that we can make with our observations is by combining results for the two analysed *s*-process elements Sr and Ba. In Fig. 14, we show [Ba/Fe] as a function of [Sr/Fe] for the bSGB, the fSGB and the halo stars. Stars with both Sr and Ba available clearly distribute

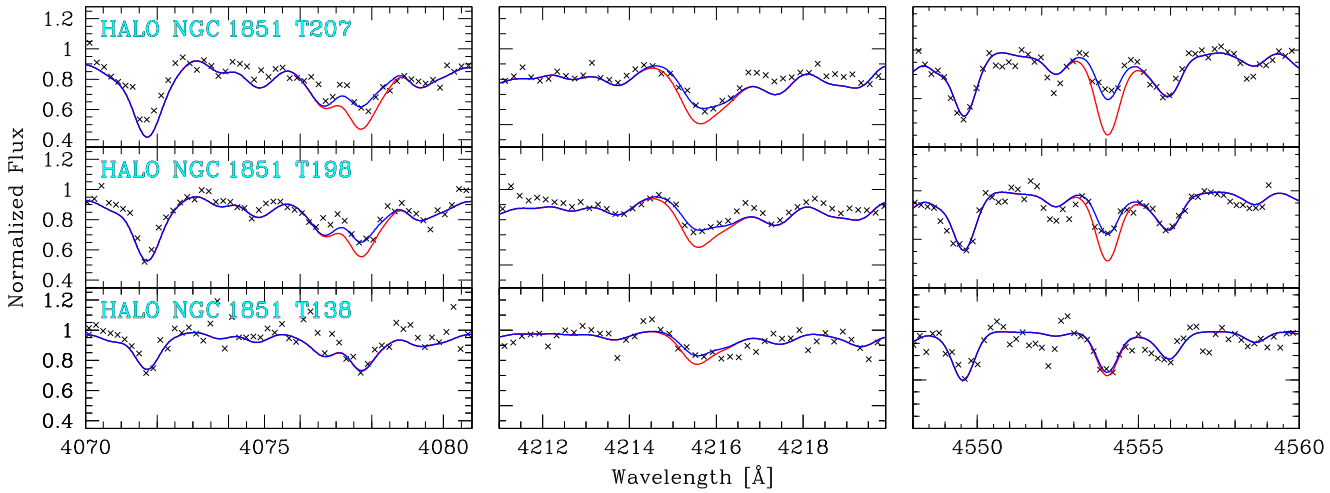

Figure 13. Some examples of observed and synthetic spectra around the measured Sr and Ba features for three NGC 1851 halo stars (T207, T198 and T138). In each panel, the points represent the observed spectrum, the blue line is the best-fitting synthesis and the red line is the syntheses computed with the mean abundances obtained for the fSGB in the NGC 1851 internal field.

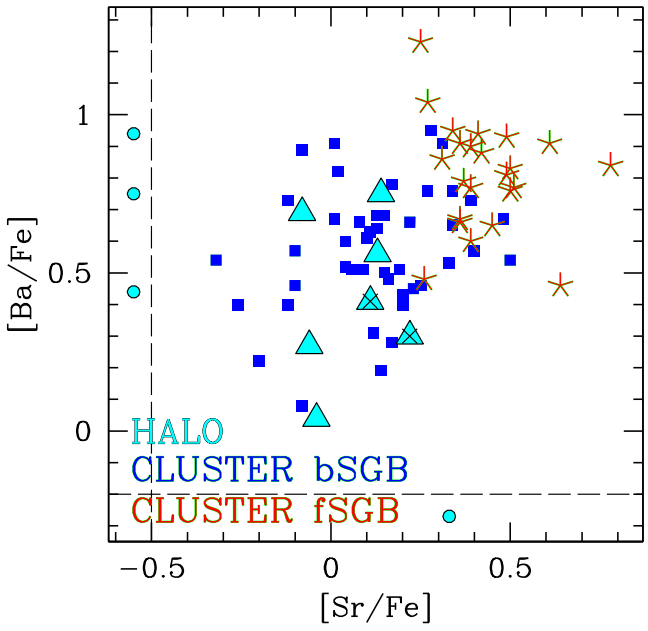

Figure 14. Barium as a function of strontium abundances relative to Fe for the NGC 1851 system: halo stars are shown as cyan triangles, cluster bSGB and fSGB have been represented in blue squares and red stars, respectively. The two halo stars with anomalous position on the CMD have been indicated with black crosses, while stars with just Ba or Sr abundance have been represented with cyan dots.

in the same manner as the bSGB stars. The two stars not lying on the NGC 1851 sequence (see Section 3.2) have been indicated with black crosses.

For completeness, in Fig. 14 we plot stars with only Sr or Ba available as cyan dots separated by the horizontal and vertical dashed lines, respectively. We comment briefly on these four stars. As previously discussed, due to the large errors in [Ba/Fe] we cannot draw conclusions on the three stars with only Ba abundances available. Indeed, the large uncertainties associated with the single Ba measurements for halo MS stars, that is about 0.29 dex as listed in Table 4, do not allow us to confidently assign the two out three stars with higher Ba to neither the *s*-rich nor the *s*-poor group. The location of the star with just Sr is inconclusive.

We can conclude that the analysis of our sample of halo stars thus does not provide strong evidence for the presence of *s*-rich stars corresponding to the fSGB population, in so far as all the stars for which Ba and Sr abundances are available have values compatible with those of the bSGB.

On the probability of observing *s*-rich stars, considering that in the central field the fSGB contributes around 35 per cent of the stars (Milone et al. 2009), we would expect to observe 1.75/5 (with Sr and Ba abundances available) at the high *s*-process composition of the fSGB. We observe no such stars. As a further test, the binomial probability of observing none out of five stars in the *s*-poor group is 0.12, and none out of seven stars (if we include the two stars with anomalous position on the CMD) is 0.05. These probabilities are small; however, we remark here that they are not zero, and future analysis of larger sample of stars is necessary to increase the sample of halo stars with available chemistry. As long as we refer to our analysed sample, the present results provide no strong evidence for the presence of *s*-rich stars, and indeed support a halo populated by just bSGB *s*-poor stars. To make this statement more conclusive, we need to improve the statistics in the future and eventually reduce our 0.12 probability to ∼0.00. For these statistics, we assume the bSGB and fSGB fractions based on *HST* and ground-based photometry from Milone et al. (2009) that follow the SGB split from the cluster centre out to 8 arcmin with no strong evidence for different radial distributions of the two branches. Beyond this distance out to the tidal radius, there are too few SGB stars to identify the sequences and determine their contribution to the total cluster mass. On the other hand, Zoccali et al. (2009) found that the fSGB dramatically drops at a distance of ∼2.4 arcmin from the centre. We note that since we have detected *s*-rich/fSGB stars up to ∼5 arcmin from the centre, we confirm that there is no drop of fSGB stars at ∼2.4 arcmin.

As abundances for Sr and Ba were possible for 7/23 stars, including two RGBs, we have 16 MS stars, including the four stars with only Sr or Ba abundance available, that do not have available abundances for both *n*-capture elements. To get chemical information for these 16 stars, we combined their observed spectra by simply averaging them with the same weight, so that we obtained a spectrum with higher S/N. Then, we constructed two MOOG synthetic spectra by averaging those corresponding to the atmospheric parameters of each star: one with the mean Sr and Ba abundances obtained for the bSGB (mean bSGB synthetic spectrum), and the other with the mean Sr and Ba of the fSGB (mean fSGB synthetic spectrum). The comparison between the mean observed halo spectrum and the mean bSGB and fSGB synthetic spectra is shown in Fig. 15. The mean observed halo spectrum near the Sr and Ba spectral features is clearly best matched by the mean bSGB synthetic spectrum. The stars not analysed for individual abundances of Sr and Ba have predominantly the bSGB abundances.

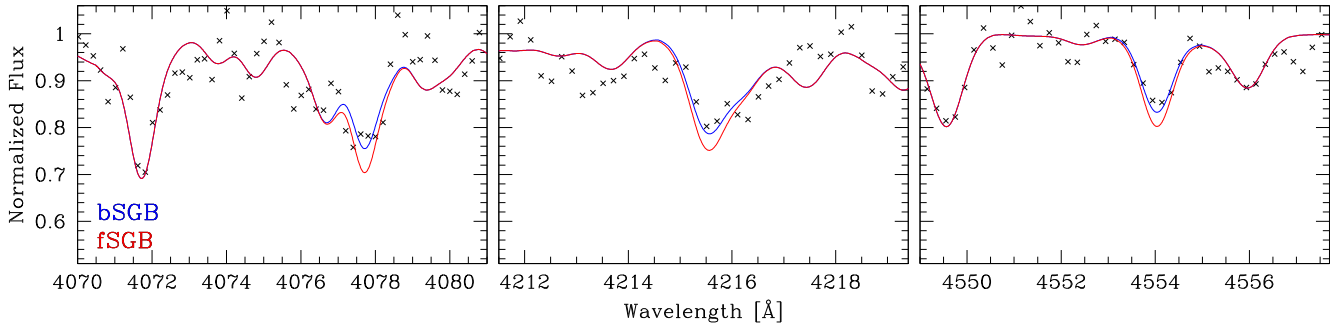

Figure 15. Observed spectrum obtained from the average of the MS halo stars for which the Sr and Ba individual abundances were not possible due to the low S/N. The observed spectrum, represented with black crosses, has been shown around the Sr (left-hand and middle panels) and Ba (right-hand panel) spectral features. The blue and red synthesis represent the average MOOG synthesis of the averaged stars for the mean Sr and Ba abundances inferred for the cluster bSGB and fSGB, respectively.

Regarding the other elements, halo chemical composition agrees with that observed in the inner field of NGC 1851. As shown in Fig. 12, the distributions of all the elements in the halo are consistent with those observed in both the bSGB and fSGB, not showing any significant difference between the abundances obtained for the two SGBs. The halo stars are enhanced in α elements Ca and Mg, and roughly solar-scaled [Cr/Fe], although the rms in this latter species is high due to observational errors. Carbon has been inferred for five stars, including T066 (not on the cluster sequence), the two red giants (T198 and T207) and two MS stars (T186 and T207). The comparison with the C abundances in the inner field can be done for just the two MS stars, as RGB stars have undergone the first dredge-up bringing carbon into the internal layers, resulting in lower surface abundances for this element. The two MS stars T186 and T220 have [C/Fe] $= -0.13$ and -0.15, respectively, and the mean differences with the median values of the internal field are Δ[C/Fe]$_{\rm (cluster-halo)} = +0.01 \pm 0.03$ dex, Δ[C/Fe]$_{\rm (bSGB\ cluster-halo)} = +0.05 \pm 0.03$ dex and Δ[C/Fe]$_{\rm (fSGB\ cluster-halo)} = -0.10 \pm 0.04$ dex, which are consistent with both the bSGB and fSGB (see Table 5).

We conclude that, for all the analysed elements, the chemical composition of the halo is consistent with that observed in the cluster (as shown in Fig. 12). In particular, the *s*-elements are consistent with the bSGB abundances. The similar abundance distribution for all the elements with available measurements is an additional signature for cluster membership and, more in general, for the existence of a halo surrounding NGC 1851.

6 THE VELOCITY DISPERSION RADIAL PROFILE

Having established the existence of a halo of stars beyond the tidal radius of NGC 1851, we can investigate the intrinsic RV dispersion ($\sigma_{\rm RV}$) of these outer stars in comparison with the inner field. To this aim, we used the procedure described in Mackey et al. (2013, see their section 4.2) that takes into account the contribution of observational errors to the RV dispersion. Briefly, we used a maximum likelihood technique, assuming that the measured RVs for our stars are normally distributed around the average value according to their measurement uncertainties and the intrinsic cluster velocity dispersion. We can obtain numerical estimates for the intrinsic cluster velocity dispersion by maximizing the logarithm of the joint probability function for the observed RVs. The procedure has been done at three different bins of radial distances from the cluster centre: namely in the central field of 3 arcmin $\times$ 3 arcmin covered by *HST* photometry, in the inner field covered by ground-based photometry at a distance from the centre between $\sim$4 arcmin and $\sim$9 arcmin, and for the stars in the outer field that covers the halo.

Fig. 16 shows the obtained intrinsic velocity dispersions in our three radial bins. In the cluster field, the velocity dispersion decreases with radius, from $\sim$5 km s^{-1} in the *HST* field to $\sim$4 km s^{-1} between 4 and 9 arcmin. There is no significant difference between the bSGB and fSGB. Scarpa et al. (2011) determined the velocity dispersion radial profile from FLAMES spectra using high-resolution setups for 184 stars along the upper SGB and the lower RGB in the inner field of NGC 1851. Their results are plotted, along with ours, in Fig. 16. Our measurements agree with those reported by Scarpa and collaborators within 1σ. Out of the tidal radius we find a dispersion comparable with that observed in the region between 4 and 9 arcmin.

We note here that some physical and technical issues may affect our $\sigma_{\rm RV}$ determination.

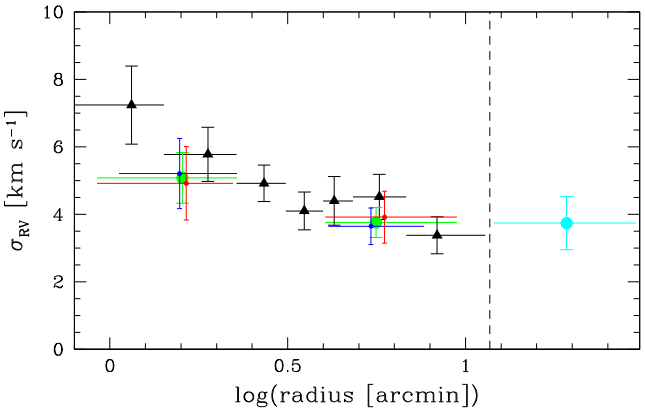

Figure 16. Intrinsic dispersions in RVs ($\sigma_{\rm RV}$) as a function of the distance from the cluster centre (in logarithmic units) for the stars in the *HST* central field (within 3 arcmin $\times$ 3 arcmin); the stars in the inner field covered by ground-based photometry (between $\sim$4 and 9 arcmin from the cluster centre) and in the outer field (from the tidal radius up to $\sim$30 arcmin from the cluster centre). The colour codes are as follows: green is for the inner field stars of NGC 1851; cyan for the halo of NGC 1851; blue and red are the stars in the inner field divided in the bSGB and fSGB samples (see Section 5.1), respectively. The black triangles are values derived in Scarpa et al. (2011). The dashed line shows the location of the tidal radius.

(i) Stellar masses: since most of the halo stars belong to the upper MS, while inner field stars are SGB, to properly compare the $\sigma_{\rm RV}$ estimates at different radial distances we need to account for the different masses of the stars. Lower mass stars should have a higher dispersion, typically, than higher mass stars. However, this effect is negligible in our sample, since the mass difference between upper MS and SGB is small. To quantify, under energy equipartition for two stars with masses m_1 and m_2, we have $\sigma_{\rm RV_2} = \sigma_{\rm RV_1} \times \sqrt{m_1/m_2}$, that for an SGB with mass $m_1 \sim 0.8$ M$_\odot$ and an MS star with mass $m_2 \sim 0.7 M_\odot$ would be $\sigma_{\rm RV_2}$ larger by $\sim$7 per cent than $\sigma_{\rm RV_1}$.

(ii) Field contamination: although we exclude that this is an issue in the inner field where we have much higher statistics, a low degree of field contamination ($\sim$2 stars out of 23) may affect our sample of NGC 1851 RV-like stars in the halo and may affect the value of $\sigma_{\rm RV}$. To estimate this effect, we determined the radial velocity dispersion ($\sigma_{\rm RV}^{i,j}$) by excluding each pair of stars (*i,j*, with $i = 1, 23$ and $j = 1, 23$) from our NGC 1851 halo sample. In the end, we obtained an average dispersion of 3.72 km s^{-1} (rms $= 0.22$) with $\sigma_{\rm RV}$ ranging from 2.57 to 3.96 km s^{-1}.

(iii) Binaries: binary contamination can inflate the dispersion. As discussed in Section 3, we do not expect a large fraction of binaries in NGC 1851 [from Milone et al. (2012) the fraction of binaries in the central field outside the half-mass radius is $\sim$1.6 per cent]. Of course, we cannot exclude that the halo stars may have, for some reason, a larger binary fraction. For the NGC 1851 halo sample, we do not see any evidence for the presence of stars whose rms in RVs from different exposures significantly exceeds that introduced by the quality of the spectra (see Section 3 for more details).

(iv) Possible fibre-to-fibre systematic errors: while the plate-to-plate systematics are randomly distributed and are likely removed using our procedure, fibre-to-fibre effects may be there as the FLAMES fibre configuration that we used is the same for every exposure (that means each star is observed with the same fibre). Such effects are small and never exceed $\sim$0.5 km s^{-1} (e.g. Sommariva et al. 2009).

With due consideration of all the issues affecting the σ_{RV} estimates, we may speculate that the apparently continuous nature of the dispersion profile from the cluster to the halo provides yet more evidence that the halo is associated with the cluster. We can also exclude a truncation in the observed σ_{RV} in the vicinity of the tidal radius, that is contrary to the expectations from King-type theoretical models. The bSGB and fSGB observed in the inner field are chemically different in the *s*-process elements, but they look kinematically similar.

7 DISCUSSION AND CONCLUDING REMARKS

We have provided a spectroscopic analysis of the halo that surrounds NGC 1851. In particular, we have studied the nature of this intriguing stellar structure by analysing RVs and elemental abundances, providing for the first time a chemical inventory in a halo surrounding a GC.

We have measured RVs and elemental abundances of Fe, C, Mg, Ca, Cr, Sr and Ba in a sample of both halo and cluster stars, from which we draw the following conclusions:

(i) the RV distribution in the observed halo field shows a peak not expected from Galactic models at the characteristic RV of NGC 1851, confirming the presence of a halo surrounding the cluster;

(ii) 15 stars in the halo field exhibit RVs and metallicities consistent with the cluster field;

(iii) our observed RV distribution agrees (apart from the RV range of NGC 1851) with that expected from Galactic models, suggesting that no other substructure, such as streams, is present in our field;

(iv) the halo has the same metallicity distribution as NGC 1851. None of the NGC 1851 RV-like stars found outside the tidal radius shows an [Fe/H] content different from the range observed in the inner field;

(v) the halo stars for which we could estimate abundances for Sr and Ba show abundances consistent with those observed on the bSGB, i.e. they have lower Sr and Ba compared with those of the fSGB;

(vi) our sample does not exhibit any strong evidence for the presence of stars with *s*-element abundances compatible with the fSGB.

Within the multiple stellar population context, qualitatively, our observations are in agreement with a scenario in which (i) the first stellar population of NGC 1851 is made up of *s*-poor (bSGB) stars; (ii) the second generation is expected to form in the central region of the cluster possibly enriched in *s*-elements; (iii) the less radially concentrated first generation is lost early in the cluster evolution due to the expansion and stripping of the cluster outer layers resulting from early mass-loss associated with first-generation supernova ejecta (e.g. D'Ercole et al. 2008). If this scenario is correct, our observations constitute the first clear evidence that GCs lose primarily first-generation stars by evaporation mechanisms. The chemical composition of field stars in the halo, that is consistent with the first-generation stars in GCs, may mainly be due to the evaporation of first-generation GC stars into the field. Although the central relaxation time of NGC 1851 is small (of the order of 10^7 yr), in the halo any dynamical time will be very long due to the low density. So, while in the central part of the cluster the time-scales are short enough that the population is mixed, in the external halo field, they are sufficiently long such that any initial gradient may have been preserved.

It is worth noting that in the CMDs shown by Milone et al. (2009) there is no obvious difference in the radial distributions of the bSGB and fSGB of NGC 1851 up to ∼8 arcmin from the centre. However, their observations are limited to a small region well within the tidal radius of the cluster, and we cannot exclude different radial gradients at more external regions. If the fSGB is more centrally concentrated and the outer parts of the cluster are dominated by the bSGB, then since outer stars are more easily lost, that would be consistent with the bSGB dominance in the halo. We recall here that both the *s*-poor and possibly also the *s*-rich groups in NGC 1851 show internal variations in light elements (e.g. C, N, O, Na). The presence of subpopulations within each main *s*-group makes the scenario more complex, challenging the identification of the sequence of the various stellar bursts that gave origin to the multiple stellar populations in this GC. An exhaustive study of the radial distributions of the NGC 1851 stellar groups should account also for the presence of these subpopulations.

The main question here is: Why does NGC 1851 possess a stellar halo with these kinematic and chemical properties? In principle, the presence of a halo may be simply consistent with a stellar system that is losing its external stars into the field. On the other hand, GCs are expected to follow a King profile, with the surface density drastically dropping at the tidal radius. It has been well established that while King models succeed in describing the internal stellar surface-brightness profiles, they often fail in the outer regions of clusters, including the Milky Way GCs (e.g. McLaughlin & van der Marel 2005; Carballo-Bello et al. 2012). GC surface-brightness profiles suggest that stellar clusters do not simply truncate on the King tidal radius, but have low-density extended haloes. All GCs should be stressed, to different extent, by interactions with the host galaxy. Hence, deviations from the King profile could not be surprising. McLaughlin & van der Marel (2005) have shown that the observed surface-brightness profiles of GCs are generally better reproduced by a modified isothermal sphere based on an ad hoc stellar distribution function developed for elliptical galaxies by Wilson (1975). The corresponding Wilson tidal radius of McLaughlin & van der Marel (2005) is larger than that derived assuming a King profile, being ∼45 arcmin for NGC 1851. However, although we can formally fit the surface-brightness profiles of GCs in the regions beyond the King radius adopting ad hoc analytical templates, in many cases it remains unclear why we observe such halo envelopes. For NGC 1851, the main question could hence not be why it possesses a halo, but why it shows such a peculiarly uniform halo, without evident tidal features in the large photometric field analysed by Olszewski et al. (2009).

The NGC 1851 halo may be a more interesting case, as it extends for 67 arcmin from the cluster centre, that is much farther than any estimate for its tidal radius present in the literature. Its very low density, as determined in Olswzeski et al., would make it easily perturbed by passages through the disc. According to Dinescu, Girard & van Altena (1999), NGC 1851 is at a distance from the galactic centre of 16.0 kpc, its orbit has apogalacticon and perigalacticon distances of ∼30 kpc and ∼5 kpc, respectively, a high eccentricity of ∼0.7 and it passes through the disc of the Milky Way five times per Gyr. Hence, it seems unlikely that an outer envelope of stars remains attached to the cluster for a Hubble time or, alternatively, that the cluster could shed sufficient stars to make such a huge envelope in half an orbit.

Our spectroscopic sample of stars does not show any evidence of tidal streams. Although our observations allow us to draw this conclusion only for a relatively small region of the halo, Olswzeski et al. did not find any evidence for tidal streams in their large field of

view. This apparent lack of streams in the Olswzeski et al. analysis is puzzling. It is difficult to envisage a scenario that assumes that such an extended low-density halo is bound to NGC 1851, if the cluster has been in an orbit around the Milky Way for a significant portion of a Hubble time. However, even if it seems unlikely, we cannot exclude that, if the cluster has been in an orbit around the Galaxy for a long time, we are seeing a particular phase of the NGC 1851 evolution: e.g. a very extended envelope of stars that is in the process of escaping from the cluster, but still bound to it. NGC 1851 is currently at an intermediate distance from the galactic centre between the apogalacticon and perigalacticon, and it is at a distance of 7.1 kpc from the Galactic plane (Djorgovski 1993), that is around the maximum distance from the plane allowed by its orbit (Dinescu et al. 1999). The halo may have formed after the last passage through the disc, and will then be largely swept away next time the cluster crosses the disc and, presumably, recreated as the cluster moves through the halo in the half-orbit time before the next disc crossing. Future dynamical simulations may be enlightening in this regard, and should prove if such a scenario is plausible for the formation of the NGC 1851 halo.

Alternatively, it is tempting to speculate that we really are seeing a system that has been captured relatively recently and the envelope does represent the former dwarf galaxy. In this case, there just have not been enough orbits yet for the envelope to be completely stripped off by passages through the disc. Hence, it is possible that the halo population could look like the first generation in the cluster in the same way as the first generation in most GCs looks like the field halo population at the same [Fe/H]. If this hypothesis is correct, then we would expect that the halo population does not host stars enriched in Na because dwarf galaxies do not show Na–O anticorrelations.

The first cluster proposed to be the nucleus of a dwarf tidally disrupted through Milky Way interactions was ω Centauri (Norris et al. 1996). Assuming a similar scenario, it would be less problematic to understand the large chemical variations, also in heavy elements, displayed by this cluster (e.g. Norris & Da Costa 1995; Johnson & Pilachowski 2010; Marino et al. 2011b). Although less pronounced, NGC 1851 shows chemical and photometric peculiarities similar to those of ω Centauri (e.g. Milone et al. 2008; Yong & Grundahl 2008; Carretta et al. 2010; Villanova et al. 2010). In contrast to NGC 1851, for the case of ω Centauri there is no evidence for stellar halo envelopes, probably because it is located relatively close to the Galactic Centre and it has a tightly bound orbit. These ensure that Galactic tidal forces at its location are relatively strong so that any loosely bound population is quickly removed preventing the survival of any such structure to the present day (see Da Costa & Coleman 2008). If the accretion of ω Centauri has not occurred recently, there has been time to remove the loosely bound outer envelope that could have originally surrounded the cluster. On the other hand, M54, which is the GC associated with the nucleus of the Sagittarius dwarf galaxy, preserves an external envelope, that is the field population of the Sagittarius. Collectively, these facts may reinforce the conjecture that *anomalous* GCs could represent the surviving nuclei of dwarf galaxies disrupted by tidal interactions with the Milky Way, and we can speculate that the halo surrounding NGC 1851 is the remnant of the parent dwarf galaxy.

To test the feasibility of this hypothesis, dynamical simulations taking into account the tidal interactions between the Milky Way and dwarfs are fundamental. Recent simulations presented in Bekki & Yong (2012) show that the halo in NGC 1851 can be reproduced if this object formed in a dwarf galaxy environment, through the merger of two clusters (corresponding to the *s*-rich and *s*-poor groups) that sink into the centre of the host galaxy. From their simulations, they expect to have three stellar populations in the halo: the *s*-poor and the *s*-rich stars, plus a third population representing the field of the host dwarf.

Our results seem to not strongly favour this idea. Assuming that each of the three populations should be equally represented in the halo, we have not found any clear evidence for the presence of either the *s*-rich stars or a third population differing from the metal distribution observed in NGC 1851 to be associated with a field population from the host galaxy. If, following the Bekki scenario, we assume that the three populations are equally represented (e.g. fSGB = 33 per cent, bSGB = 33 per cent and field = 33 per cent), the probability to not observe any star with the Ba and Sr abundances of the fSGB population of NGC 1851, even if not null, is low (see Section 5.2). This suggests that, even with our modest statistics, it is unlikely that there are three populations equally represented in the field, as in the Bekki & Yong scenario.

Furthermore, even if an internal metallicity variation of the order of 0.10 dex in the halo (that we cannot see because of observational errors) cannot be ruled out, the metal distribution of the external field (15 stars) is very similar to that observed within the tidal radius. This favours the idea that the halo does not host stellar populations with metallicities too distinctive with respect to NGC 1851, but we cannot completely exclude that the lack of such stars is instead introduced by photometric selection effects that can affect our sample. We note that Olswzeski et al. found evidence for the presence of at least the two SGB populations (bSGB and fSGB) in the CMD of the NGC 1851 halo. However, it is possible that their fSGB may not correspond to the one observed in the cluster, given that they found a significantly larger separation between the two SGBs than that found out to 8 arcmin from the cluster centre (Milone et al. 2009).

As previously discussed, the halo population we are actually observing could be either the *s*-poor population observed in the cluster or the field population of the host galaxy, which may show the same metallicity and chemical properties of the cluster bSGB. In the latter case, we do not have to see Bekki & Yong's postulated third population, as it may be the same as the cluster first generation and we may have to look at a lot of halo stars to see a different [Fe/H] distribution from that of the cluster first generation. It is also worth noting that the dynamical simulations by Bekki & Yong assume that NGC 1851 is the result of a merger between two clusters. It might be interesting to see if similar simulations assuming the NGC 1851 various groups formed in a self-pollution scenario are able to better reproduce the observations.

The lack of a drop in the velocity dispersion profile is another piece of evidence that makes NGC 1851 hardly compatible with the King model. A similar lack is intriguingly seen in M54, the GC lying at the centre of Sagittarius. This GC shows a velocity dispersion profile that falls off with the distance from the cluster centre, and increases outside, due to either contamination from Sagittarius in the external part of the cluster or to tidal harassment from the host galaxy (Bellazzini et al. 2008). In the hypothesis that the NGC 1851 halo represents the parent galaxy population, we would qualitatively expect a relatively high velocity dispersion for the halo. On the other hand, if the halo is simply formed by stars evaporating from NGC 1851, it may be that the stars in the region outside the tidal radius are undergoing some kind of heating, due to either tides and/or unseen (dark) matter or modified Newtonian dynamics. We are not able to answer this question here. We only note that, according to dynamical simulations presented in Küpper et al. (2010), the velocity dispersion of unbound escaping stars outside GC tidal radii

should significantly increase flattening due to tidal interactions with the Milky Way. The orbit of NGC 1851 suggests that it is not at its perigalacticon and it is at its largest distance from the Galactic plane, but according to Küpper et al. this effect, even if magnified at the perigalacticon, seems to be present at any location on the orbit. We note however that our sample of 23 stars outside the tidal radius may still be bound to the cluster. Future investigations on the velocity dispersions in the halo of NGC 1851 may give information on the nature of the NGC 1851+halo system, assuming that measurements will be available at different radial locations in the halo and with better statistics.

We conclude that the presence of such an extended halo in NGC 1851 may suggest that the complex chemical enrichment in this GC has taken place in a dwarf whose nucleus is NGC 1851. Interestingly, the location of NGC 1851 coincides with the disc of satellites, a relatively thin, highly inclined plane defined by the distribution of luminous Milky Way satellite galaxies (Kroupa, Theis & Boily 2005; Metz, Kroupa & Jerjen 2007; Pawlowski, Pflamm-Altenburg & Kroupa 2012; Pawlowski & Kroupa 2013). It would be interesting in the future to see whether NGC 1851 is co-orbiting with this structure or not.

It is conceivable that NGC 1851's host galaxy was tidally disrupted by the collision and its stars were dispersed into the Milky Way halo in a way similar to what we observe with M54 and the Sagittarius dwarf today. The ultra-low-density halo of NGC 1851 could therefore be the last trace of its ancient host. Our spectroscopic analysis provides, for the first time, chemical abundances from low-resolution data and the identification of two low RGB halo stars lying on the fiducial of NGC 1851, which may be useful to follow-up at higher resolution. The present analysis is confined to a relatively small sample, which does not show strong evidence for *s*-enrichment. We stress however that in the future, we need to extend this analysis to larger fields to increase the statistics and possibly confirm the lack/deficiency of fSGB stars in the halo that result from the present study.

ACKNOWLEDGEMENTS

We warmly thank the referee Christian Moni Bidin for his helpful comments that improved the quality of the paper. The authors thank M. Pawlowski for useful discussions. AFM, AD and MA have been supported by grants FL110100012 and DP120100991. APM, HJ, GDC and JEN acknowledge the financial support from the Australian Research Council through Discovery Project grant DP120100475. LS acknowledges the support by Project IC120009 "Millennium Institute of Astrophysics (MAS)" of Iniciativa Científica Milenio del Ministerio de Economía, Fomento y Turismo de Chile.

REFERENCES

Alonso A., Arribas S., Martínez-Roger C., 1999, A&AS, 140, 261
Alves-Brito A., Yong D., Meléndez J., Vásquez S., Karakas A. I., 2012, A&A, 540, A3
Anderson J., Bedin L. R., Piotto G., Yadav R. S., Bellini A., 2006, A&A, 454, 1029
Anderson J. et al., 2008, AJ, 135, 2055
Arlandini C., Käppeler F., Wisshak K., Gallino R., Lugaro M., Busso M., Straniero O., 1999, ApJ, 525, 886
Bekki K., Freeman K. C., 2003, MNRAS, 346, L11
Bekki K., Norris J. E., 2006, ApJ, 637, L109
Bekki K., Yong D., 2012, MNRAS, 419, 2063
Bellazzini M. et al., 2008, AJ, 136, 1147
Bellini A., Bedin L. R., Piotto G., Milone A. P., Marino A. F., Villanova S., 2010, AJ, 140, 631
Bessell M., Murphy S., 2012, PASP, 124, 140
Carballo-Bello J. A., Gieles M., Sollima A., Koposov S., Martínez-Delgado D., Peñarrubia J., 2012, MNRAS, 419, 14
Cardelli J. A., Clayton G. C., Mathis J. S., 1989, ApJ, 345, 245
Carretta E. et al., 2010, A&A, 520, A95
Cassisi S., Salaris M., Pietrinferni A., Piotto G., Milone A. P., Bedin L. R., Anderson J., 2008, ApJ, 672, L115
Castelli F., Kurucz R. L., 2004, preprint (astro-ph/0405087)
Collet R., Asplund M., Nissen P. E., 2009, PASA, 26, 330
D'Ercole A., Vesperini E., D'Antona F., McMillan S. L. W., Recchi S., 2008, MNRAS, 391, 825
Da Costa G. S., Coleman M. G., 2008, AJ, 136, 506
Da Costa G. S., Held E. V., Saviane I., Gullieuszik M., 2009, ApJ, 705, 1481
Da Costa G. S., Held E. V., Saviane I., 2014, MNRAS, 438, 3507
Djorgovski S., 1993, in Djorgovski S. G., Meylan G., eds, ASP Conf. Ser., Vol. 50, Physical Parameters of Galactic Globular Clusters. Astron. Soc. Pac., San Francisco, p. 373
Dinescu D. I., Girard T. M., van Altena W. F., 1999, AJ, 117, 1792
Foreman-Mackey D. T., 2010, PhD thesis, Queen's Univ.
Gallagher A. J., Ryan S. G., García Pérez A. E., Aoki W., 2010, A&A, 523, A24
Gallart C. et al., 2003, AJ, 125, 742
Gilmore G. et al., 2012, The Messenger, 147, 25
Goldsbury R., Richer H. B., Anderson J., Dotter A., Sarajedini A., Woodley K., 2011, AJ, 142, 66
Gratton R., Sneden C., Carretta E., 2004, ARA&A, 42, 385
Gratton R. G., Villanova S., Lucatello S., Sollima A., Geisler D., Carretta E., Cassisi S., Bragaglia A., 2012, A&A, 544, A12 (G12)
Gray R. O., Corbally C. J., 1994, AJ, 107, 742
Han S.-I., Lee Y.-W., Joo S.-J., Sohn S. T., Yoon S.-J., Kim H.-S., Lee J.-W., 2009, ApJ, 707, L190
Harris W. E., 1996, AJ, 112, 1487
Hauschildt P. H., Allard F., Baron E., 1999a, ApJ, 512, 377
Hauschildt P. H., Allard F., Ferguson J., Baron E., Alexander D. R., 1999b, ApJ, 525, 871
Hill V. et al., 2002, A&A, 387, 560
Ibata R. A., Gilmore G., Irwin M. J., 1994, Nature, 370, 194
Johnson C. I., Pilachowski C. A., 2010, ApJ, 722, 1373
Kappeler F., Beer H., Wisshak K., 1989, Rep. Prog. Phys., 52, 945
Kauffmann G., White S. D. M., Guiderdoni B., 1993, MNRAS, 264, 201
King I., 1962, AJ, 67, 471
Klypin A., Kravtsov A. V., Valenzuela O., Prada F., 1999, ApJ, 522, 82
Koch A., Grebel E. K., Odenkirchen M., Martínez-Delgado D., Caldwell J. A. R., 2004, AJ, 128, 2274
Kraft R. P., 1994, PASP, 106, 553
Kroupa P., Theis C., Boily C. M., 2005, A&A, 431, 517
Küpper A. H. W., Kroupa P., Baumgardt H., Heggie D. C., 2010, MNRAS, 407, 2241
Lardo C. et al., 2012, A&A, 541, A141
Lardo C. et al., 2013, MNRAS, 433, 1941
Lee J.-W., Kang Y.-W., Lee J., Lee Y.-W., 2009, Nature, 462, 480
Lodders K., 2003, ApJ, 591, 1220
Mackey A. D., Da Costa G. S., Ferguson A. M. N., Yong D., 2013, ApJ, 762, 65
Marino A. F., Villanova S., Piotto G., Milone A. P., Momany Y., Bedin L. R., Medling A. M., 2008, A&A, 490, 625
Marino A. F., Milone A. P., Piotto G., Villanova S., Bedin L. R., Bellini A., Renzini A., 2009, A&A, 505, 1099
Marino A. F. et al., 2011a, A&A, 532, A8
Marino A. F. et al., 2011b, ApJ, 731, 64
Marino A. F. et al., 2012a, A&A, 541, A15
Marino A. F. et al., 2012b, ApJ, 746, 14
Mashonkina L., Zhao G., 2006, A&A, 456, 313
McLaughlin D. E., van der Marel R. P., 2005, ApJS, 161, 304
Metz M., Kroupa P., Jerjen H., 2007, MNRAS, 374, 1125
Milone A. P. et al., 2008, ApJ, 673, 241

Milone A. P., Stetson P. B., Piotto G., Bedin L. R., Anderson J., Cassisi S., Salaris M., 2009, A&A, 503, 755
Milone A. P. et al., 2012, A&A, 540, A16
Moni Bidin C. et al., 2011, A&A, 535, A33
Moore B., Ghigna S., Governato F., Lake G., Quinn T., Stadel J., Tozzi P., 1999, ApJ, 524, L19
Norris J. E., Da Costa G. S., 1995, ApJ, 447, 680
Norris J. E., Freeman K. C., Mighell K. J., 1996, ApJ, 462, 241
Norris J. E., Bessell M. S., Yong D. et al., 2013, ApJ, 762, 25
Odenkirchen M. et al., 2001, ApJ, 548, L165
Olszewski E. W., Saha A., Knezek P., Saha A., Knezek P., Subramaniam A., de Boer T., Seitzer P., 2009, AJ, 138, 1570
Pasquini L. et al., 2002, The Messenger, 110, 1
Pawlowski M. S., Kroupa P., 2013, MNRAS, 435, 2116
Pawlowski M. S., Pflamm-Altenburg J., Kroupa P., 2012, MNRAS, 423, 1109
Piotto G. et al., 2012, ApJ, 760, 39
Robin A. C., Reylé C., Derrière S., Picaud S., 2003, A&A, 409, 523
Ryan S. G., Norris J. E., Beers T. C., 1999, ApJ, 523, 654
Sarajedini A. et al., 2007, AJ, 133, 1658
Sbordone L., Salaris M., Weiss A., Cassisi S., 2011, A&A, 534, A9
Scarpa R., Marconi G., Carraro G., Falomo R., Villanova S., 2011, A&A, 525, A148
Schlegel D. J., Finkbeiner D. P., Davis M., 1998, ApJ, 500, 525
Simmerer J., Sneden C., Cowan J. J., Collier J., Woolf V. M., Lawler J. E., 2004, ApJ, 617, 1091
Simmerer J., Ivans I. I., Filler D., Francois P., Charbonnel C., Monier R., James G., 2013, ApJ, 764, L7
Smith V. V., Suntzeff N. B., Cunha K., Gallino R., Busso M., Lambert D. L., Straniero O., 2000, AJ, 119, 1239
Sneden C., 1973, ApJ, 184, 839
Sollima A., Gratton R. G., Carballo-Bello J. A., Martínez-Delgado D., Carretta E., Bragaglia A., Lucatello S., Peñarrubia J., 2012, MNRAS, 426, 1137 (S12)
Sommariva V., Piotto G., Rejkuba M., Bedin L. R., Heggie D. C., Mathieu R. D., Villanova S., 2009, A&A, 493, 947
Stetson P. B., 2000, PASP, 112, 925
Stetson P. B., 2005, PASP, 117, 563
Trager S. C., Djorgovski S., King I. R., 1993, in Djorgovski S. G., Meylan G., eds, ASP Conf. Ser. Vol. 50, Structure and Dynamics of Globular Clusters. Astron. Soc. Pac., San Francisco, p. 347
Ventura P., Caloi V., D'Antona F., Ferguson J., Milone A., Piotto G. P., 2009, MNRAS, 399, 934
Villanova S., Geisler D., Piotto G., 2010, ApJ, 722, L18
Wilson C. P., 1975, AJ, 80, 175
Yong D., Grundahl F., 2008, ApJ, 672, L29
Yong D., Grundahl F., D'Antona F., Karakas A. I., Lattanzio J. C., Norris J. E., 2009, ApJ, 695, L62
Yong D. et al., 2014, MNRAS, 441, 3396
Zoccali M., Pancino E., Catelan M., Hempel M., Rejkuba M., Carrera R., 2009, ApJ, 697, L22

SUPPORTING INFORMATION

Additional Supporting Information may be found in the online version of this article:

Table 2. Coordinates, basic photometric data and RVs for the NGC 1851 halo and cluster (inner field) stars.
Table 3. Adopted atmospheric parameters and chemical abundances for the NGC 1851 halo and cluster (central field) stars (http://mnras.oxfordjournals.org/lookup/suppl/doi:10.1093/mnras/stu1099/-/DC1).

Please note: Oxford University Press is not responsible for the content or functionality of any supporting materials supplied by the authors. Any queries (other than missing material) should be directed to the corresponding author for the paper.

This paper has been typeset from a TEX/LATEX file prepared by the author.